IZMIR KATIP CELEBI UNIVERSITY ★ GRADUATE SCHOOL OF NATURAL AND APPLIED SCIENCES

DEVELOPMENT OF MWCNT NANO-COMPOSITE MATERIALS AS GAS SENSOR

M.Sc. Thesis

Uğur ACAR

Material Science and Engineering Programme

Thesis Advisor: Assoc. Prof. Dr. Şerafettin DEMİÇ

FEBRUARY-2017

**IZMIR KATIP CELEBI UNIVERSITY ★ GRADUATE SCHOOL OF
NATURAL AND APPLIED SCIENCES**

**DEVELOPMENT OF MWCNT NANO-COMPOSITE MATERIALS
AS GAS SENSOR**

M.Sc Thesis

Uğur ACAR
(130111035)

Material Science and Engineering Programme

Thesis Advisor: Assoc. Prof. Dr. Şerafettin DEMİÇ

FEBRUARY-2017

Uğur ACAR, a M.Sc. student of İzmir Katip Çelebi University student ID Y130111035, successfully defended the thesis entitled "DEVELOPMENT OF MWCNT NANO-COMPOSITE MATERIALS
AS GAS SENSOR", which he prepared after fulfilling the requirements specified in the associated legislations.

Thesis Advisor: **Assoc. Prof. Dr. Şerafettin DEMİÇ**   ....
Izmir Katip Celebi University

Jury Members: **Prof. Dr. SunaTİMUR**   ....
Ege University

Assoc. Prof. Dr. Fethullah GÜNEŞ   ....
Izmir Katip Celebi University

Teslim Tarihi   :   **13 Şubat 2017**
Savunma Tarihi   :   **28 Şubat 2017**

To my family,

ACKNOWLEDGEMENT

TABLE OF CONTENTS

x

x

ABBREVIATIONS

CO	: Carbon monoxide
CO$_2$	: Carbon dioxide
O$_2$	: Oxygen
QCM	: Quartz Crystal Microbalance
VB	: Valance Band
CB	: Conduction Band
IDE	: Interdigitated Electrode
FET	: Field Effect Transistor
SAW	: Surface Acoustic Wave
SiO$_2$	: Silicium dioxide
MHz	: Megahertz
PPM	: Per part million
PPB	: Per part billion
SCCM	: Standard Cubic Centimeters per Minute
CoFe$_2$O$_4$COOH	: Cobalt Ferrite
Fe$_3$O$_4$COOH	: Acid Functionalized Iron (III)
MWCNT	: Multi-Walled Carbon Nanotube
FT-IR	: Fourier Transform Infrared Spectra
AC	: Alternating current

LIST OF TABLES

LIST OF FIGURES

xvi

DEVELOPMENT OF MWCNT NANO-COMPOSITE MATERIALS

AS GAS SENSOR

SUMMARY

Besides human health, toxic gases are harmful for both animal and plant health. Various concentrations cause so many fatal or permanent problems. Therefore, controlling toxic gases (carbon monoxide, carbon dioxide), and oxygen at the indoor environment is of vital importance. In this study, effect of gold nanoparticle doping on the gas sensing properties of chitosan-based conductive polymers were investigated via acoustic wave and electrical based techniques. In this study, quartz crystal microbalance technique was used. Quartz Crystal Microbalance is a powerful technique for nano scale determination of the sorption properties of materials. According to Sauerbrey relation, the mass change on quartz crystal electrode cause a certain shift in the resonant frequency of a vibrating crystal oscillator. This shift can be monitored using QCM method.

Being easily supplemented, synthesized, modified with different kinds of functional groups and improved gas sorption properties, conducting polymers are suitable for gas sensors. Chitosan, $Fe_3O_4COOHMWCNT$ derivatives and $CoFe_2O_4COOHMWCNT$ derivatives were synthesized this study. A series containing chitosan-based materials doped with nanoparticles were formed..

Modification of chitosan with $CoFe_2O_4COOHMWCNT$ 4% caused the sensitivity of the $CoFe_2O_4COOHMWCNT$ 2% material fell down with respect to bare but increased with respect to bare chitosan.

Modification of chitosan with $Fe_3O_4COOHMWCNT$ 4% caused the sensitivity of the $Fe_3O_4COOHMWCNT$ 2% material fell down with respect to bare but increased with respect to bare chitosan. From the results show that chitosan, $CoFe_2O_4COOHMWCNT$ 2% , $CoFe_2O_4COOHMWCNT$ 4% , $Fe_3O_4COOHMWCNT$ 2% and $Fe_3O_4COOHMWCNT$ 4% are selective to CO with respect to the other gasses.

ÇOK DUVARLI KARBON NANOTÜPLER İLE NANOKOMPOZİT MALZEMELERİN GAZ SENSÖRÜ OLARAK GELİŞTİRİLMESI

ÖZET

Toksik gazlar insan sağlığının yanında hem hayvanların hem de bitkilerin sağlığı için zararlıdır. Farklı konsantrasyonlar sağlık üzerinde çeşitli kalıcı veya ölümcül problemlere yol açarlar. Bu yüzden ortamdaki toksik gazların (karbon monoksit, karbon dioksit, amonyak) ve oksijenin ortamdaki kontrolü hayati önem arz etmektedir. Bu çalışmada, altın nanoparçacık katkılamanın pirol tabanlı iletken polimerlerin gaz algılama özelliklerine olan etkisi akustik dalga tekniği ve elektriksel ölçüm yöntemleriyle incelenmiştir. Bu çalışmada, kuartz kristal mikrobalans metodu kullanılmıştır. Kuartz kristal mikrobalans, nanogram mertebesinde, malzemelerin gaz tutma özelliklerini inceleyebileceğimiz bir tekniktir. Sauerbrey ilişkisine göre, kristal elektrotundaki kütle değişimi, titreşen kristal elektrotta belirli bir frekans kaymasına neden olur. Bu değişim QCM metodu ile ölçülebilir.

İletken polimerlerin kolayca katkılanabilmesi ve sentezinin kolay olması ayrıca kolayca farklı fonksiyonel grupların bağlanabilmesi ile gaz adsorplama özellikleri iyileştirilebilir olması gaz sensor uygulamaları için uygun malzemelerdir. Bu çalışmada chitosan, $Fe_3O_4COOHMWCNT$ türevleri ve $CoFe_2O_4COOHMWCNT$ türevleri sentezlenmiştir. Nanopartiküllerle katkılanmış kitosan esaslı materyaller içeren bir seri oluşturuldu.

Bu çalışmada, çitosan temelli olarak sentezlenmiş ve asit fonksiyonelleştirilmiş kobalt ferit ve demir (III) oksit nanokatkılanmış olan malzemelerden seri oluşturulmuştur. Çitosan, kobalt ferit ve türevleri,ve demir (III) oksit ve türevleri çalışmada kullanılmıştır.

$CoFe_2O_4COOHMWCNT$ 4% ile Kitosan'ın modifikasyonu
$CoFe_2O_4COOHMWCNT$ 2% maddesinin duyarlılığına göre düşmesine neden olurken sadece kitosana göre artmıştır.
$Fe_3O_4COOHMWCNT$ 4%ile Kitosanın modifikasyonu $Fe_3O_4COOHMWCNT$ 2% maddenin duyarlılığına göre düşmesine neden olurken, saf kitosan ile karşılaştırıldığında artmıştır. Elde edilen sonuçlara göre, diğer gazlara göre, Kitosan, $CoFe_2O_4COOHMWCNT$ 2%, $CoFe_2O_4COOHMWCNT$ 4%, $Fe_3O_4COOHMWCNT$ 2% ve $Fe_3O_4COOHMWCNT$ 4% CO için seçici olmaktadır.

1. INTRODUCTION

We live in chemical air environment- natural and artificial- and some include a variety of other important gases which are harmful to life [1]. Figure 1.1 illustrates typical concentration levels of the respective gas components. Nowadays, air pollution caused by increasing industrial jobs (toxic and combustible gases in particular) poses a great threat to human life. From time to time, man-made gases inevitably occur near industrial facilities, and are potentially hazardous for both employees and other residents. Those undesired incidents worldwide include asphyxiation, explosions and loss of life. Therefore, gas sensors play an important role in helping prevent the above-mentioned problems, in various modern technological processes and controlling of the gas analysis [1-3]. Gas detector enable us to know that there is a hazardous gas leakage in our environment by giving alarm with sound. Thus, thanks to gas sensors, we can prevent accidents due to the gas leaks and save lives and equipments. Gas detectors are used to detect flammable and combustible gases. Such a device may be located in various locations including oil wells, gas containers and gas trunk pipelines.
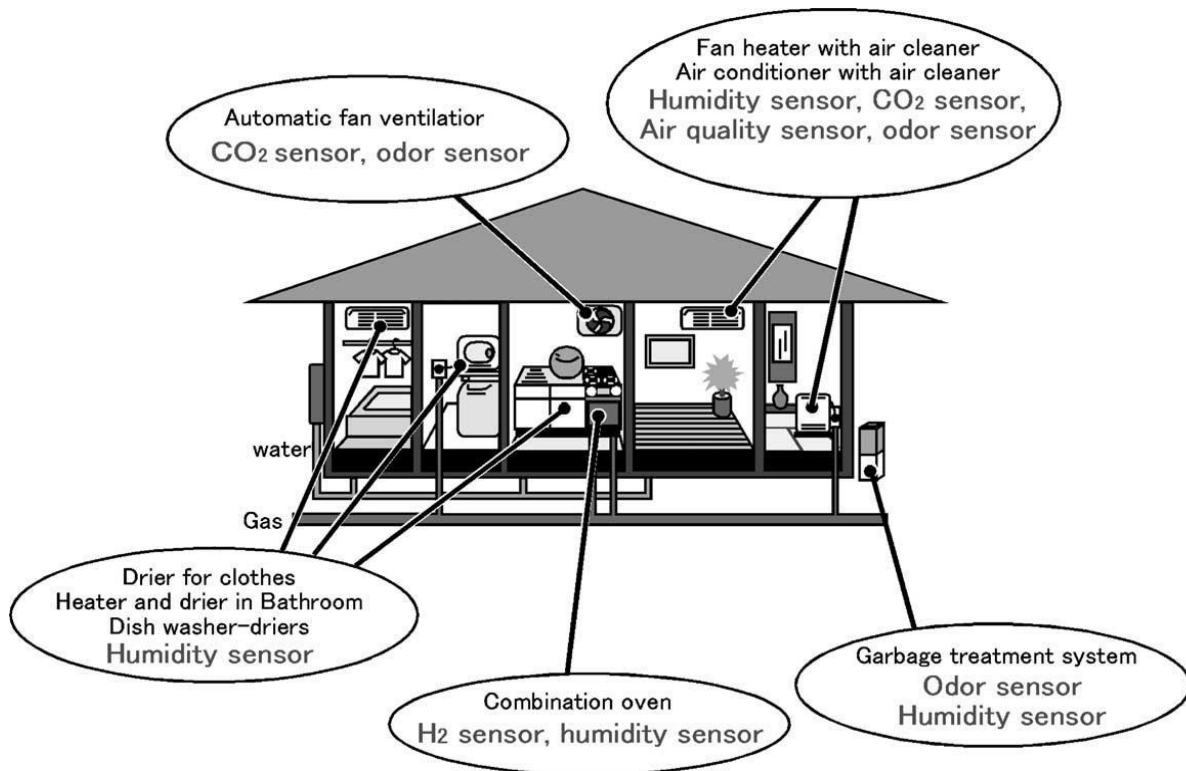
Figure 1.1 Different types of gas sensors equipped in a house [4].

Gas sensors operating in a wide area have certain properties which are precision, selectivity, response time, accuracy, resolution, sensitivity, reproducibility and linearity [5-7]. In this context, the most abundant in natural nanoparticles is chitosan. Chitosan is easily obtained in nature and is a polymer and has a cheap cost. It is obtained from chitin. Chitin has hydroxymethyl functional group while chitosan has amideion.In this study, carbon monoxide (CO), carbon dioxide (CO_2) and oxygen (O_2) were used. Properties, sources and impact of these gases except O_2 are shown in the Table1.1

Table 1.1: Properties of toxic gases used in thesis

Gases	Features	Sources	Effects
CO_2	Colorless, odorless and nontoxic gas	burning animals, cement production, breathing people, including motorized vehicles and industry, especially energy production	Greenhouse gases in the atmosphere. To create a lack of oxygen and may cause suffocation or smothering
CO	Colorless, odorless, flammable, non-irritating, very poisonous	gas, coal or wood as fuel is produced by incomplete combustion. Vehicle exhaust.	It restricts blood's oxygen transport capability. A small amount of dizziness, headache, fatigue, and makes slow response times. A reduced ability to exercise. Fetuses, infants and pregnant women are more vulnerable to the effect. Those effects are lethal.

Quartz crystal microbalance (QCM) is an acoustic wave technique exploiting the properties of the piezo electric effect. An AC voltage is applied across the piezoelectric quartz crystal. Crystal goes at its own resonant frequency, normally 10 MHz and 30 MHz [8]. The three-dimensional waves produced travel across the entire bulk of the crystal, resulting in an increase in the total mass of the crystals when exposed to various gases. Gas molecules accumulates on the surface and are absorbed by the thin film material. This added mass changes the resonance frequency of the quartz crystal and is used for the detection of gas.

In this thesis, polymers chitosan-based nanoparticles were used to detect the sensitivity of CO, CO_2 and O_2. The sensitivity were investigated via acoustic waves and electrical-based techniques against those gases. Gas-interacted electrodes -especially electronic armored and airtight- were designed to obtain electrical signals and are conducted to QCM in a measuring cell. CO, CO_2 and O_2 were sent thin-film-coated electrodes. Concentration levels of those gases ranged from 0 vol% to 100 vol%, by increasing 5 intervals serially of controlled using mass flow meter connected computer. By means of the changes on the natural resonance frequency as a result of thin-film-coated QCM vibrating, gas absorption was measured. These changes were then converted to mass sorbed Sauerbrey relation.

Gas Sensor

A gas sensor is a device that detects the presence of gases in an area and also they can be used as the interior to determine whether there is gas leak in the environment. They are devices that convert the physical or chemical fluctuation into electrical signal and after that this signal can be easily interpreted. This type of equipment is used to detect a gas leak and controlled with a control system interface, so a process can be

automatically shut down. A gas sensor can sound an alarm to operators in the area where the leak occurs, giving them the opportunity to evacuate [9-27]. This type of device is important because there are many gases that can be harmful to organic life, such as humans or animals[28-42].

1.1.1. Characteristic of ideal gas sensors

A gas sensor that works properly should have the following features;

*Sensitivity; Analytical precision of the measured signal and the concentration unit is defined as the ratio between the change. In other words, the slope of this graph defines the calibration.

*Selectivity; means that whether the gas sensor can respond and analyze some exact specifications.

*Stability is defined by the ability of any gas sensor's response to replication the same result for a certain period of time.

* Detection limit is the detection by the gas sensor under a certain condition and at a certain temperature, the gas concentration is defined as the minimum ratio.

* Dynamic range is defined as the range between the lowest and the highest rate of the gas concentration.

* Linearity, this means that the concentration of gas readings are in direct proportion to the electrical.

* Resolution is the minimum amount that a gas sensor can separate in the gas concentration.

* Recovery time is the time that a gas sensor returns to the initial state by a value after a certain concentration gradient.

*Response time is defined as the time a gas sensor reaches from zero to a certain value.

* **Working temperature**, is the temperature from which the data comprising a maximum result with the best conditions.

Those are critically important features of a gas sensor. These features of a gas sensor determine the quality and functionality.

An ideal gas sensor should provide all of the features mentioned above. However, this will be expensive and it is almost impossible that a gas sensor has all those features. In real life, since it will be costly and unnecessary to produce a perfect gas sensor, it will make more sense to produce a gas sensor according to the purpose. For example, in a gas sensor, response time will be very important for the industry while detection limit level is ppm. The environmental gas sensor detection limit to be made at that time will be very important and sensitization will become very important in this sense. If this is done according to the purposes of the gas sensor, the transport features will be more significant than both cost and reusability.

Types of gas sensors

There are many different ways in making the gas sensors using different materials and based on different principles.

1.1.2.1 Field effect transistor (FET) gas sensors

Semiconductor materials change the conductivity of the materials used on demand. This process can be controlled by only one type of charge. This field effect transistors (FET) is based on the operating principle. FET devices allow us to detect the electric current through chemical and physical changes. FET type transistors is for work areas which are especially designed. MOSFET is needed for gas sensor application. There are three fundamental elements on a FET device; source, drain and gate. Silisium oxide

is generally used as a semiconductor material in the FET operating principle. A signal is obtained from the material which is placed in between source and drain. When the signal is sent from the source to drain and the I-V characteristic is investigated, we can easily see the characteristics of the material. The variety of the signal depends on the gas concentration environment.
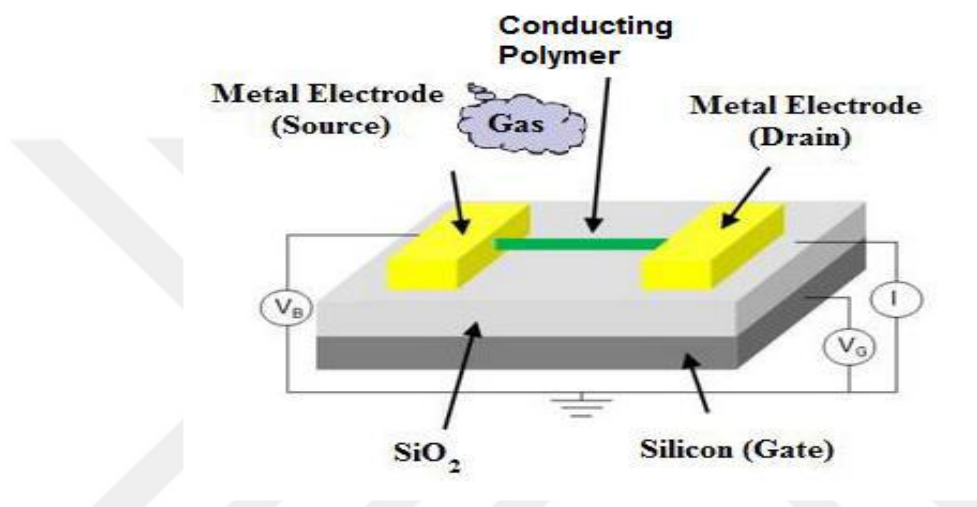
Figure 1.2 Basic structure of FETs [48].

1.1.2.2 Optical gas sensors

Optical gas sensors is often considered as the simplest version of sensors. Such gas sensors are durable due to their high stability, sensitivity and selectivity. Optical gas sensors are usually applied in chemistry and biology. Response time is quite short, which makes it important on this issue. Besides, environmental changes, such as catalyst poisoning incidents, do not have an impact on the performance of optical gas sensors. The working principle is simply based on spectroscopy. However, its size and manufacturing cost limit their extensive usage. As a conclusion, not so many optical gas sensors are manufactured due to their limited market share[49].
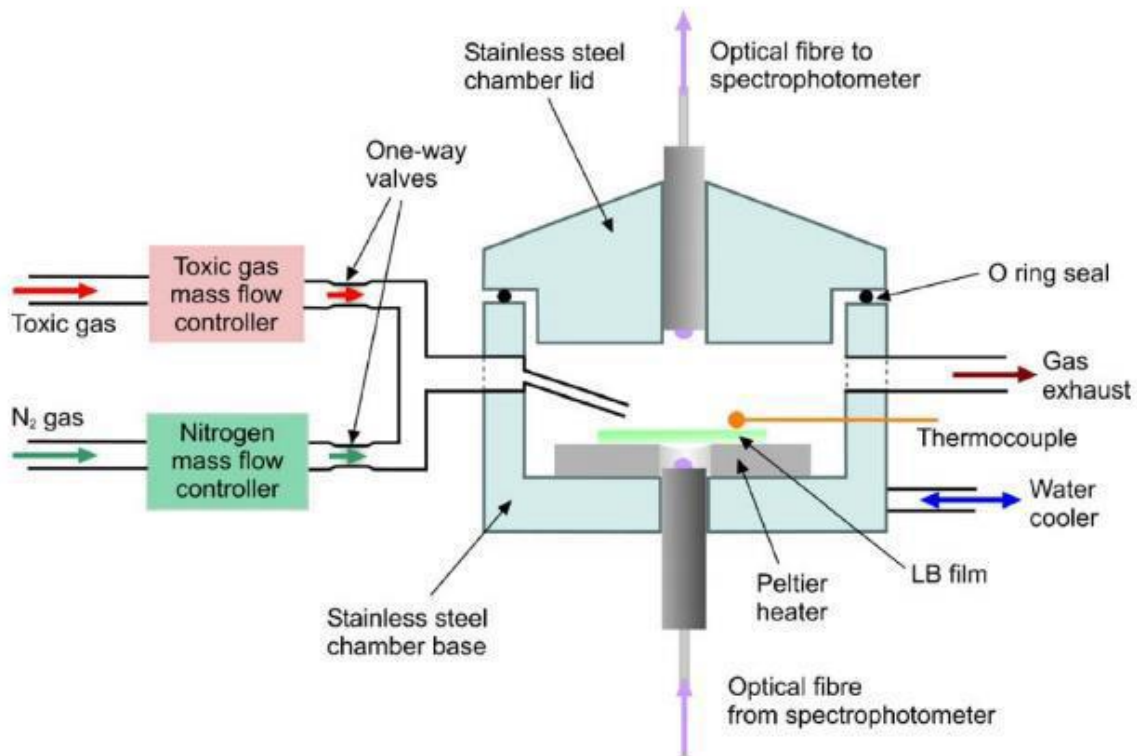
Figure1.3 An optical gas sensor system.

1.1.2.3 Semiconductor gas sensors

Semiconductor gas sensors are found abundant in the field due to their low-cost and high-efficiency in sensitivity. These gas sensors are also referred to as metal oxide semiconductor gas sensors due to their structure. They basically separate target gases via redox reaction between gas and oxide surface at temperatures exceeding 200° C [50].

The operation principle of this sensor type is explained in two steps [51]: Firstly, the redox reaction happen between the aimed gas and the surface on which the O- is distributed. As a consequence, variation emerges on the oxide surface. Secondly, this variation is transformed into electrical signal so that it can be observed as sensor output. This variation may be determined in terms of capacitance, mass, work function,

reaction energy and optical properties [52]. Furthermore, the redox reactions occur between the temperature of about 200 to 250° C.
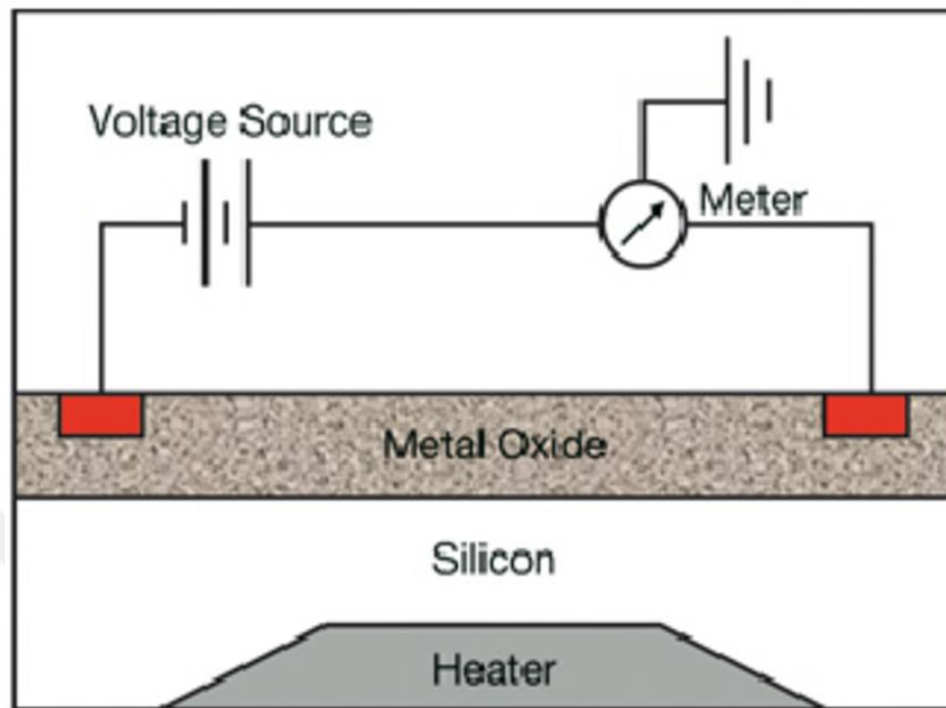
Figure1.4 Basic components of metal oxide based semiconductor gas sensor [53].

1.1.2.4 Electrochemical gas sensors

Electrochemical gas sensors are often used to detect oxygen and toxic gases. Electrochemical gas sensors are made of gold or platinum as the basis for an electrolyte fuel cells, where the electrolyte used is an aqueous solution of strong acid. When a cell detects gas, a slight current is generated in direct proportionate to the gas concentration. Basically, an electrochemical gas sensor is composed of diffusion barrier, a counter-electrode (cathode), a sensing electrode (working electrode, anode) and an electrolyte. When there is no chemically reactive gas in the surrounding air, oxygen diffuses into the cell and adsorbs on both electrodes. In theory, although no current is expected, still a very slight current flow can be observed between the electrodes. As a result of this, a stable potential voltage between the electrodes occurs.

Depending on the gas type, oxidation or reduction of the gas emerges as the gas penetrates through the barrier, generating a current flow because of the potential difference between the two electrodes.
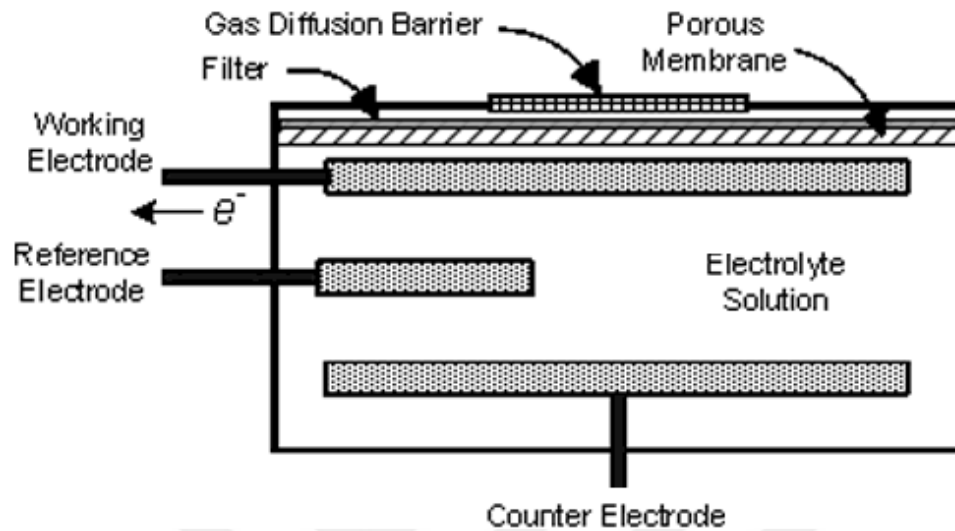
Figure1.5 Basic construction of electrochemical gas sensor [54].

1.1.2.5 Catalytic gas sensors

In the last decade, catalytic gas sensors are widely demanded and used. This sensor type has a platinum wire strapped around a permeable ceramic carriage. Catalytic sensors consists of a coiled platinum wire coil into ceramic pellets. A catalyzer, mostly platinum or palladium, is spread on the ceramic carriage surface so that the methane gas can burn. The sensor temperature is maintained as the same level of the catalyzer surface in order to oxidize the methane when a voltage strikes the methane gas continuously. When the methane is combusted by the catalyzer on the surface, the emerging energy increases the sensor temperature, resulting an increase in the resistance of the platinum heater. The amount of released energy and increase in the resistance of the platinum heater are directly proportional to the amount of methane or other hydrocarbon-based explosive combustible gases in the air. This sensor type is

preferred in the fields where hydrocarbon-based gases are used because of their high selectivity towards those gases.
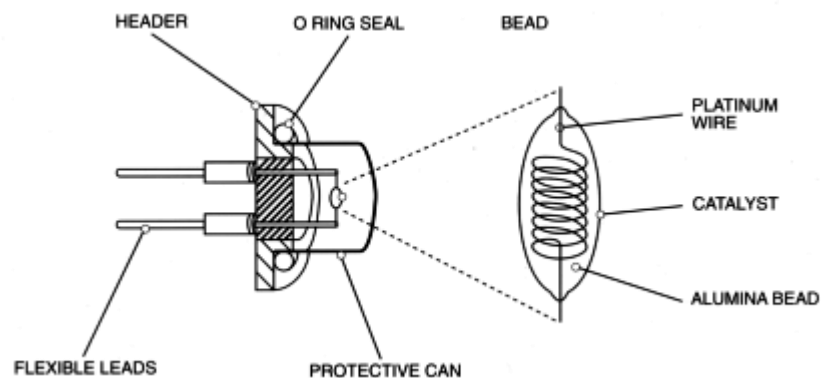
Figure1.6 Basic construction of catalytic gas sensor [55].

1.1.2.6 Piezoelectric gas sensors

Piezoelectric sensors are classified into two groups; SAW and QCM. QCM generates a wave and that waves goes through the bulk of sensor. SAW sensors generate surface waves and those waves move surface of sensors. Working principles of both sensors are the same. When the mass of piezoelectric gas sensor coated with sensing material changes because of a gas adsorption, a variation occurs in resonant frequency [56].

1.2. Theoretical Foundations

1.2.1. Piezo-electric effect and quartz crystal microbalance theory

The piezoelectric effect, literally was defined by Currie brothers 'Pierre and Jacques' for the first time in 1880. Currie brothers ascertained that tourmaline, quartz and potassium sodium tartrate have crystal structures that produce electrical reaction because of the stress and strain applied at specific directions. In contrast to this effect, materials, such as quartz, mechanically deforms when electrical signals are applied.

The results of mechanical deformation is in direct proportion to the applied electric field intensity [57]. Despite the fact that the resulting voltage and the magnitude of the force are very minor, piezoelectric sensors are widely used. Piezoelectric materials are frequently encountered in submarine sonar sensor applications. Piezoelectric materials can be classified into two main groups; first ceramic material and second in crystal materials.

Crystal structures show natural piezoelectric effects; ceramic materials, on the other hand, also known as piezo-ceramics, show artificial piezoelectric effects. The most well-known piezo-ceramic materials are known as barium titanium ($BaTiO_3$) and lead zirconate titanate (PZT). While the Curie temperature of $BaTiO_3$ is 120 °C, Curie temperature of PZT is between 150 °C and 200 °C.

The piezoelectric effect can be used as a mass sensor, which was put forward for the first time by Sauerbrey. Modifies in the mass of material deposited on the crystal surface cause the shift of crystal's resonance frequency. Sauerbrey discovered that crystal frequency shifts are uncorrelated with the physical properties of the deposited material [58].

Mass alterations on the crystal can be observed via basic measurement techniques for the frequency shift, even though we do not have much knowledge about the physical properties of the deposited material. QCM technique, depending upon fundamental physic principles, is applied in many fields, such as thin film coating, gas sensors, thickness monitor, and many other. In this technique, frequency shift of the QCM electrode coated with gold thin film is measured. The thickness of thin films was used to be measured by QCMs in 1960s and 1970s. Basically, the QCMs may be used just as gas sensors, where sensitive receptor installed on the electrode senses the gas leak [59, 60]. Quartz crystal is one of the most abundant minerals in the nature and is used

as an oscillator in this process. Quartz is, in fact, pure silisium dioxide (SiO2). Its melting point is 1650 °C and specific weight is 2.65 g/cm^3. When silisium dioxide is heated up to 573 °C, which is its transition temperature, the structure of crystal changes. If crystal structure is formed above the transition temperature, Quartz is named as beta-quartz and if it is formed in the rest temperature, it is called alpha-quartz. In resonator application, only alpha-quartz is preferred due to its superiority in terms of piezoelectric and mechanical properties.
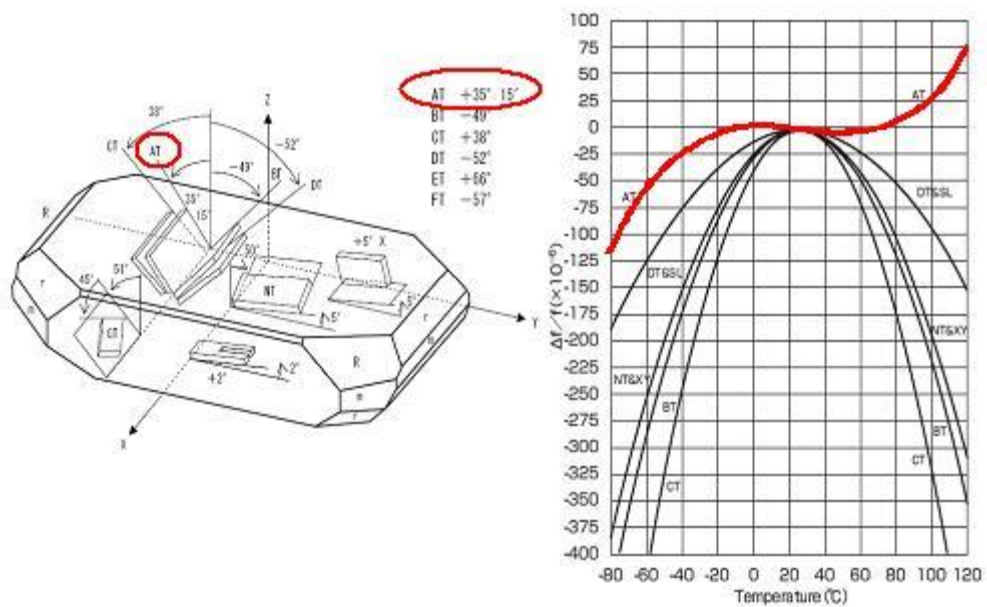
Figure 1.7 Different quartz crystal cut angels [61].

The cutting angle in the production effects the vibration frequency of the quartz crystal which is to be used as resonator. The quartz's vibration is determined by the cutting angle in accordance with the selected application requirements. Generally, AT cutting, BT cutting, SC cutting, IT cutting, FT cutting are most widely used for various application purposes. In the thickness shear mode, AT-cut crystals are generally used

for QCM electrodes and oscillates. AT cutting quartz crystal is cut at the magnitude of angle 350° 5′, 350° 10′ or 350° 15′ in regard to pure quartz crystal's Z axis.

The frequency of the chosen crystal oscillators for gas sensor applications are generally between 5 MHz and 30 MHz. High-frequency quartz crystals require thinner crystals, however it makes them more fragile. It is given below how resonance frequency varies with temperatures for different cut angles of pure quartz. In many cases, AT-cut quartzes are cut at an angle 35°15′ with regard to y-z axis. Electronic equipments generate heat between 500 °C and 600 °C. Since AT-cut quartz has the less temperature coefficient, it is considered more suitable for those temperatures. AT-cut quartzes with 35° 10' angle are more commonly preferred for detection. The temperature coefficient for this kind of quartzes is almost zero between temperatures 0 °C and 500 °C.
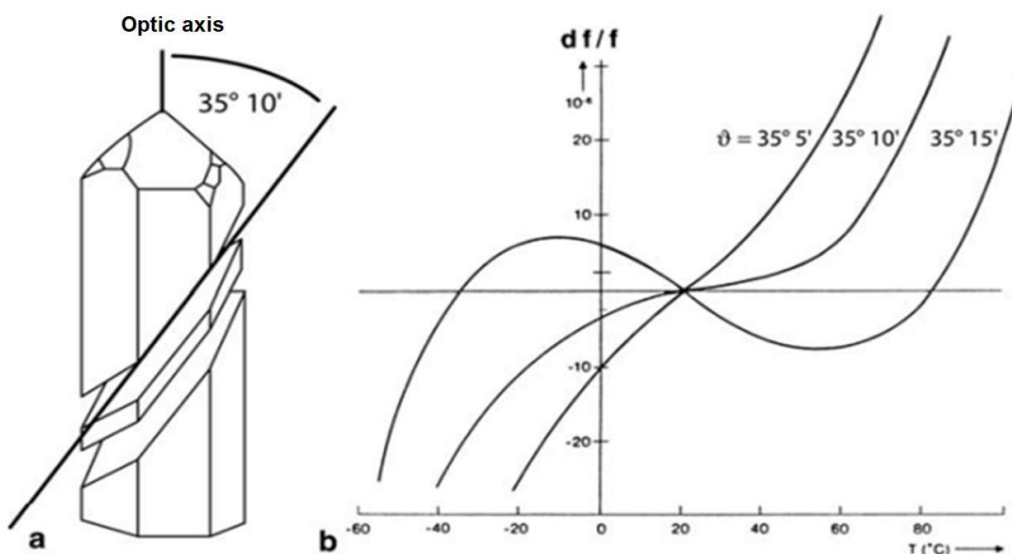
Figure1.8 Quartz crystal's (a) AT-cutting angle and (b) natural vibration frequency, temperature and cutting angle relation [62,63].

Due to the cutting properties, AT-cut quartz is the best option for QCM applications [64]. In the QCM method, oscillators which are disc shaped and between 5 MHz and

30 MHz, are often used. Vibration frequency (f_R) is determined depending on the crystal thickness. Gold electrode on the both sides of the QCM electrode, either produced with lithographic or vacuum deposition methods, does not interact with oxygen or receptor materials. In order to trigger the acoustic waves, QCM electrodes are used. Receptor chemical material that is to interact with the gas analyte is coated as thin film on these electrodes by using any coated method.
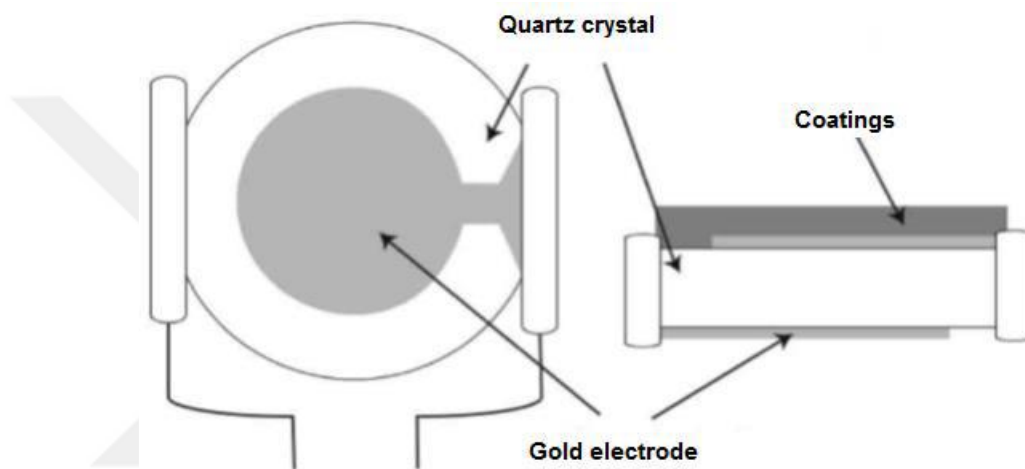
Figure1.9 Quartz Crystal Microbalance gold electrode.

M means mass and t means thickness. At the resonance condition, wavelength λ:

$$\lambda = \frac{2t}{n} \qquad (1.1)$$

For n=1 frequency (f) and for higher harmonics n value is bigger than one, so shear velocity v is defined as:

$$v = \lambda f \qquad (1.2)$$

frequency is equal to:

$$f = \frac{v}{2t} \qquad (1.3)$$

With the help of a very small change in the thickness of resonance frequency, shift can

be found by differentiation on both sides of the above equation.
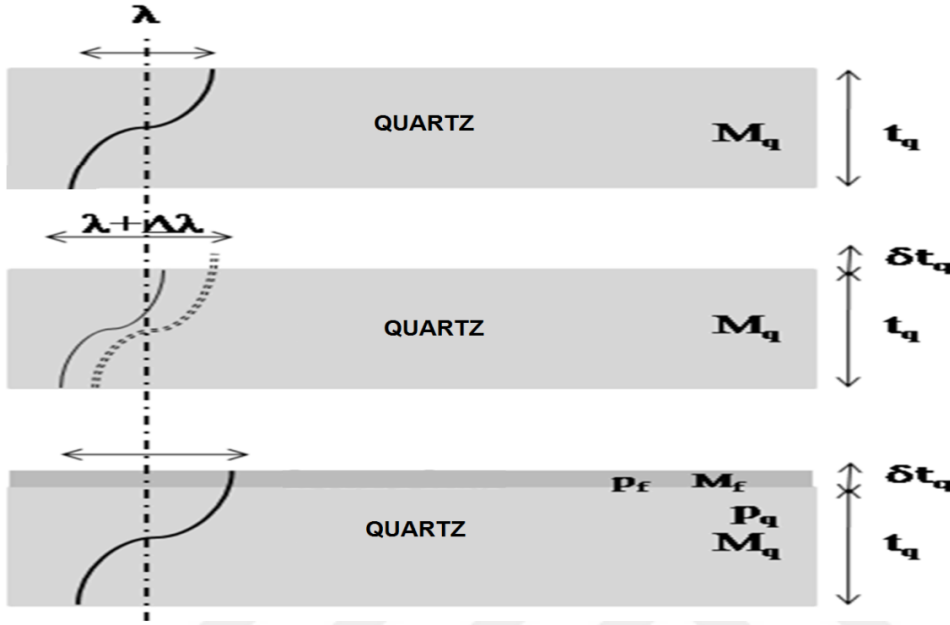
Figure1.10 The wave advancement of thin-film-coated quartz crystal electrode.

So

$$dF = -\frac{v}{2t^2} dt \qquad (1.4)$$

We will find relative change if we divide above equation by than above one

$$dF = -\frac{dt}{t} \qquad (1.5)$$

For this reason, in the above manner, the relative thickness of the crystal resonant

frequency change is reduced. Mass M per unit area coated material and the amount of

change in mass per unit area in ΔM are written as:

$$\frac{\Delta F}{F} = -\frac{\Delta M}{M} \qquad (1.6)$$

The net change in mass ΔM was assumed co-distributed over the surface area in this

derivation. Therefore, changes in mass per unit area is proportional to the change of

all mass ΔM crystal over the crystal surface, which means that the shear rate is the same over the entire crystal surface. M and ΔM are written in terms of the density of materials per area on the thin film (ρ_f) and in terms of thickness (t_f). Relative change in resonance frequency:

$$\frac{\Delta F}{F} = -\frac{\rho f t_f}{\rho t} \qquad (1.7)$$

The resonance frequency $F = v/2t$ is put in proper place in the above equation:

$$\frac{\Delta F}{F} = -\frac{2F\rho f t_f}{v\rho} \qquad (1.8)$$

Or we can show in a different way:

$$t_f = \frac{\Delta F v \rho}{2F^2 \rho f} \qquad (1.9)$$

found.

F, ρ, and v values are constants as result of production of electrode. This equation says that if the density of coated material is known, QCM will be used as a thickness monitors.

We can find crystal constant

$$C_q = \frac{2}{v\rho} \qquad (1.10)$$

So the relationship between the frequency offset and mass

$$\Delta F = -C_q F^2 \Delta M \qquad (1.11)$$

can be written.

Consequently , the changes in resonant frequency

$$\frac{\Delta F_p}{F} = C_q F \Delta M_f \qquad (1.12)$$

In the end, the equations becomes its final version. The following equation is known as the Sauerbrey equation. Derivations of this equation in different ways are also possible. Change on the stored material on crystal can be determined only by measured resonance frequency shift without dependence on the material's physical properties. Thus, it is shown that the frequency change is directly related to changes in mass.

$$\Delta f = \frac{2f_0^2}{A\sqrt{\mu\,\rho}}\Delta m \qquad (1.13)$$

Here, natural vibration frequency of QCM crystal is f_0. A is the area of coated gold on QCM crystal. μ is the quartz shear stress and ρ describes the density of the crystal. Sauerbrey equation was developed to confirm only vibration properties of coated solid material on electrode in air condition.

QCM measurements were carried out in the gas phase only until 1980, but as of 1985 the work was done in the first liquid phase and it was proved that QCM electrode is capable of vibrating steadily in an entirely fluid-filled environment. The resonance frequency shift as a result of the work done in the liquid environment was found to be proportional to the fluid density multiply viscosity.

1.2.2. Non-linear (Positive) QCM response

Sauerbrey stated that an interaction between the absorbed material and analyte leads to decrease in frequency and negative frequency shifts on QCM electrode [62]. On the other hand, in some cases, sensing materials display a positive frequency in spite of the fact that they adsorb gases. It can be described as the visco-elastic changes in the mechanical stiffness of the sensing material.

Sauerbey equation defines this relation between the mass of sorbed materials on the QCM surface and the frequency shifts of the quartz crystals. Notwithstanding,

Sauerbey equation is only applicable when the adsorbed material's mass is much lower than the starting frequency of electrode and the mass which is deposited on the quartz crystal surface which oscillates with the quartz at the same frequency. Coated oscillating film has to have the same wave velocity along with the quartz crystal surface. Sauerbrey equation indicates a linear relationship between the frequency shifts and mass increase, neglecting the physical properties of the deposited films. Mass on the films increases while QCM frequency decreases. However, in some situations, non-linear behaviors can be observed [66-68]. Actually, minor perturbations in the mechanical and physical characteristics of deposited film or the material on quartz crystal may cause non-linear or positive responses in resonance frequency of the quartz crystal. Hunt et al.[95-97] puts forward the existence of an equation from time-dependent perturbation theory in order to explain the positive QCM frequency as;

$$t\frac{\partial \Delta w}{\partial t} + \Delta w = \frac{w_u h_f}{\pi\sqrt{\boldsymbol{\rho}_q \mu_q}}X\left[-w_u\left(\Delta\boldsymbol{\rho} - \frac{\Delta\mu}{\boldsymbol{V_s^2}}\right) + j\left(\frac{\partial \Delta \boldsymbol{\rho}}{\partial t} - \frac{1}{V_s^2}\frac{\partial \Delta \mu}{\partial t}\right)\right] \qquad (1.14)$$

Where h_f is the film thickness, ρ_q is mass density of quartz crystal, *Vs* is acoustic wave velocity across the deposited film section, ρ is density of film, and μ_q is shear stiffness of quartz, μ is the stiffness of the thin film, Δ is difference between perturbed and unperturbed quantities, and subscript u is used to identify unperturbed quantities. Assuming $\Delta\rho$, $\Delta\omega$, and $\Delta\omega$ are constant with time and omitting kinetic changes, Equation 1.15 can be rearranged as following;

$$\Delta f = -\frac{2f_u^2 h_f}{\sqrt{\rho_q \mu_q}}\left(\Delta\rho - \frac{\Delta\mu}{V_s^2}\right) \qquad (1.15)$$

Since μ and ρ are constant, the mass uptake can be defined as $\Delta m = \Delta\rho Ahf$ (*A* being the sensing area), the first term of Equation 1.15 is the Sauerbrey equation which covers

static changes in mechanical stiffness of deposited film. This relation correlates a negative frequency shifts with the attached mass on QCM sensor (first term), whereas a positive frequency response to mechanical stiffness of the film (second term). Another effect which causes a deviation from the Sauerbrey equation might result from liquid clusters formed by the condensation on the coated quartz crystal. In this situation, an initial drop in the frequency shift is accompanied by a subsequent increase due to the liquefaction of the adsorbate.

1.2.3. Adsorption kinetics

Adsorption process is caused by the case of low energy molecular physics. This low energy level is an active field comprising the combination of adsorbed molecules. The literature describes in detail the adsorption phenomena [76]. The solid's surface is composed of identical active fields that will be accommodated by active species which is denoted as 's'. After adsorption, the following notation will be used if it is considered as a real chemical reaction;

[A] represents a compound A in gaseous state

$\ll$ A $\gg$ is for a constituent A in a solid or gas environment,

$<$ A $>$ is for a pure solid or gas phase of compound A.

In this case, the adsorption reaction is written as:

$$[G] + \ll s \gg \Leftrightarrow \ll G-s \gg$$
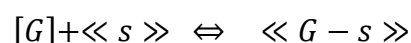
$\ll$G-s$\gg$ is the new species formed, G-s will exist in gas concentration 's'.

1.2.4 Thermodynamic model of the Langmuir adsorption isotherm

If the mass flow law is applied to the adsorption equilibrium reaction;

$$K = \frac{|\ll G - s \gg|}{P|\ll s \gg|} \tag{1.16}$$

in here K is constant of equilibrium. We can define it ;

$$K = K_0 \, exp\left(-\frac{\Delta H^\circ}{RT}\right) \tag{1.17}$$

Adsorption is an exothermic process, attended with a negative enthalpy change (ΔH° < 0). A negative value for ΔH° means that if the temperature increases the overturn reaction occurs. Thus, adsorption is favored at low temperatures.

In an ideal solution, if S represents the number of free sites, S_0 means the number of sites, and θ point out the fraction of sites that are in use, which is expressed as;

$$\theta = \frac{S_0 - S}{S_0} = |\ll G - S \gg| \tag{1.18}$$

then;

$$|\ll s \gg| = \frac{S}{S_0} = 1 - \theta \tag{1.19}$$

which yields,

$$K = \frac{\theta}{(1 - \theta)P} \tag{1.20}$$

and,

$$\theta = \frac{KP}{1 + KP} \tag{1.21}$$

"Langmuir isotherm" name given to this correlation points out the percentage coverage of the surface as a homographic function of pressure. This function is a suitable relation to describe most adsorption-related experimental results. An important perspective of this relation is that, at low surface coverage fractions (θ << 1), a proportionality law- similar to Henry's law- is obtained where $\theta = KP$.

1.2.5. Langmuir–Blodgett Technique

Langmuir-Blodgett technique, we simply want to tell that it is based on insoluble polymer on a substrate with a hydrophilic surface as it is raised from the liquid covered by this polymer monolayer [69-70]. It is also possible to immerse a substrate with a hydrophobic surface in water covered by a polymer monolayer and then slowly draw it back out. The biggest advantage of the Langmuir-Blodgett technique is that we can obtain a conceivable depositing ordered films with known and controlled thickness (in the range ±2.5 nm).

In this principle, we can use prepare mono- and multi-molecular layers and architectures with high perfection, different layer symmetries, and molecular orientations. Despite such beneficial properties, this method is not very effective especially to use in chemical gas sensor technology in real terms. On the one hand, when we take usable kinds of polymer for this method into consideration, they appear to be limited in terms of variety. In case of metal oxide, there are two accepted approaches for planar waveguide fabrication [71] . First one is, the substrate material is modified, e.g., by ion exchange in SiO_2 or $LiNbO_3$[72-74]. For example, titanium metal can be diffused into lithium niobate or lithium tantalate substrates. The additional impurities cause a required change in refractive index. Second one is, a waveguide layer is deposited on top of a substrate material (coating), as is done with metal oxides or nitrides [75,76] . Here, high refractive index waveguides can be achieved more easily, but often they are poriferous and lack adequate chemical resistance [76].

1.3 Materials

MWCNT was provided from Cheap-Tube Inc. from USA. Ferric chloride hexahydrate and ferrous chloride tetrahydrate were purchased from Fluka and used without further purification. All other chemicals were of analytical grade and were used without further purification. Materials used in this thesis was synthesized by Dr. Mehmet Şenel at Fatih University. chitosan was purchased commercially [77].

1.3.1 Multiwall-carbon nanotube/cobalt ferrite hybrid

Fourier transform infrared (FT-IR) spectra were recorded in transmission mode with a Perkin Elmer BX FT-IR infrared spectrometer. The powder samples were ground with KBr and they were compressed into a pellet. FT-IR spectra in the range 4000-400 cm^{-1} were recorded so as to investigate the nature of the chemical bonds which are formed [77].
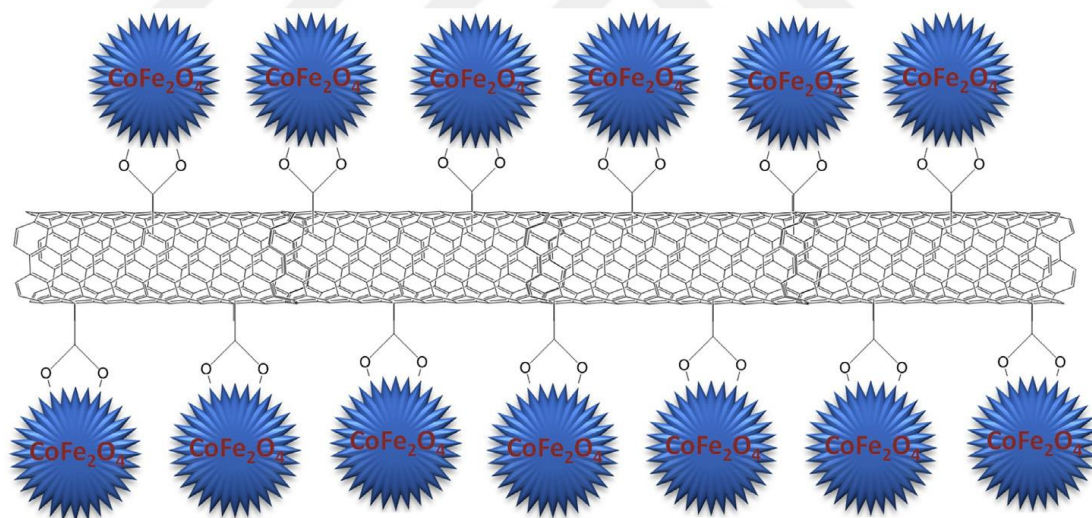
Figure 1.11. Simplified representation of the preparation of MWCNT-COOH/$CoFe_2O_4$ hybrid [77].

After oxidation with a mixture of H_2SO_4 and HNO_3, the peak at 1680 cm^{-1} which is associated with the asymmetric $C - O$ stretching band of the carboxylic acid (-COOH) (Fig.1.12 (a)). A peak at 1083 cm^{-1} is attributed due to C-O bond stretching

and the band at 1580 cm^{-1} results from the $C = C$ double bonds. 2910 and 2847 cm^{-1}

peaks are due to symmetric and asymmetric stretching of C-H and is indicative of the

presence of aliphatic $-CH_2$ groups [78]. The binding of $CoFe_2O_4$ NPs to o-MWCNTs

was confirmed by FT-IR as shown in Fig. 1.12(b).
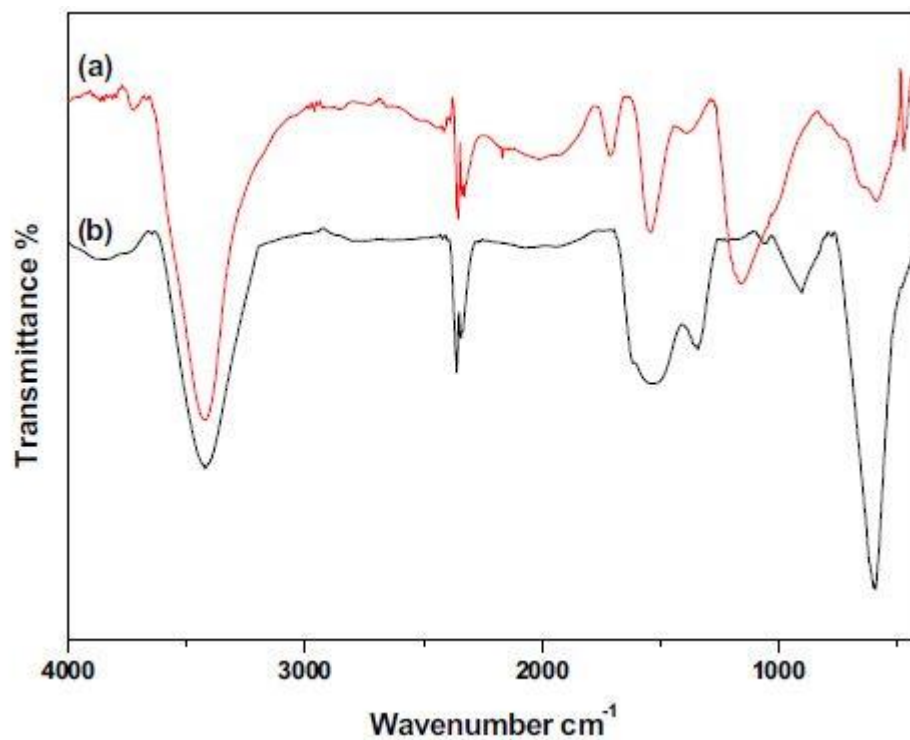
Figure 1.12 FT-IR spectra of (a) MWCNT-COOH and (b) MWCNT-COOH/$CoFe_2O_4$

hybrid.

1.3.2 Acid Functionalized Multiwall Carbon Nanotube/Magnetite Hybrid

A functionalized multiwall carbon nanotube (MWCNT)–COOH/Fe_3O_4 hybrid was manufactured by co-precipitation method. Fe_3O_4 Nanoparticles were attached stably to the surface of the carboxyl groups (COOH) [79].
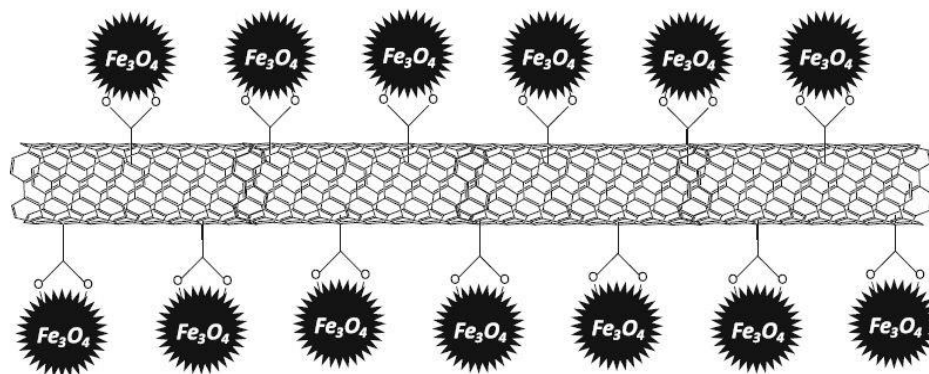
Figure 1.13 Simplified schematic representation for the manufacturing of MWCNT–COOH/Fe$_3$O$_4$ hybrid [79].

FT-IR was used to characterize the molecular structure of MWCNT–COOH/Fe$_3$O$_4$ hybrid and pre-oxidized MWCNT:FT-IR spectra of pristine and surface oxidized MWCNTs (MWCNT−COOH) are shown in Fig. 1.14. The characteristic bands due to generated polar functional groups on the MWCNT are observed in the FT-IR spectrum of the MWCNTs after chemical oxidation in H_2SO_4 / HNO_3 . These can be listed as follows: v_{OH}= 3,433cm^{-1}; $v_{C=o}$= 1,706 cm^{-1}; $v_{Hbonded(C=0)}$= 1,635 cm^{-1}; $v_{C=C}$= 1,570 cm^{-1}; and v_{C-C-C}= 1,180 cm^{-1} [80-84]. A characteristic peak of MWCNTs at 1,570 cm^{-1}ascribed to C=C bonding is present in the FT-IR spectrum of MWCNT–COOH/Fe$_3$O$_4$ hybrid, while the absorption band observed at 592 cm^{-1} is associated with the Fe−O stretching vibrations related to the presence of magnetite nanoparticles [83, 84]. The disappearance of C=O vibrations and appearance of two other absorptions at slightly lower wave number, due to symmetric and asymmetric

stretching of O−C−O, reveals the conjugation of NPs to the MWCNT surface via bridging interactions [85].
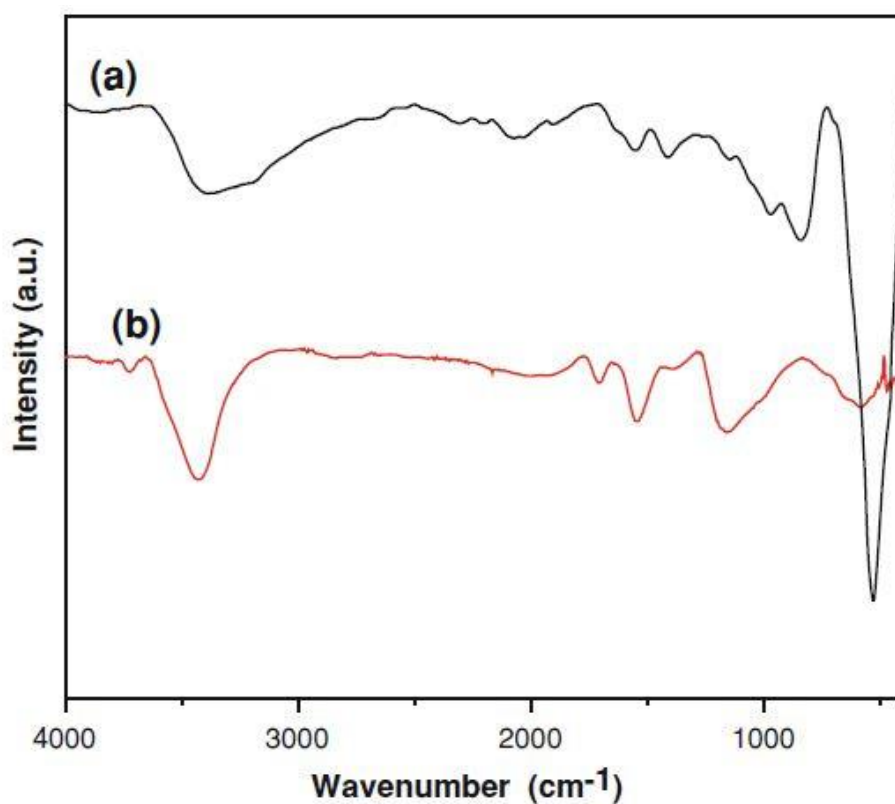
Figure 1.14 FT-IR spectrum of (a) MWCNT–COOH/Fe_3O_4 hybrid and (b) MWCNT–COOH [85].

1.3.3 Chitosan

Chitosan is a linear polysaccharide composite of randomly distributed β-(1-4)-linked D-glucosamine (deacetylated unit) and N-acetyl-D-glucosamine (acetylated unit). It is made by treating the chitin shells of shrimp and other crustaceans with an alkaline substance, such as sodium hydroxide.

Chitosan can dissolve in 0.1M acetic acid (at 60 degrees Celsius. 5 hrs. with stirring). The reaction lasted on at 60 degrees Celsius for five hours.
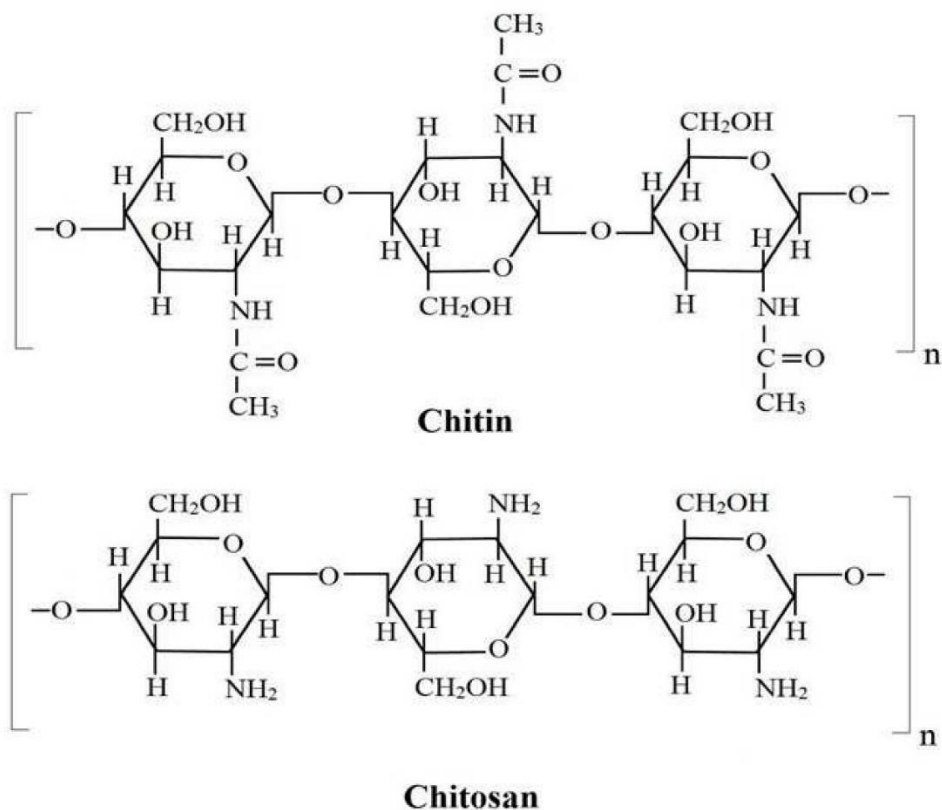
Figure 1.15 Schema of Chitin and Chitosan [86].

1.3.4 Chitosan - Multiwall-carbon nanotube/cobalt ferrite hybrid

$CoFe_2O_4COOH - MWCNT - $ chitosan solutions (0.1 mg/ml) were prepared in 1% acetic acid solution and were stirred at room temperature overnight. Chitosan and $CoFe_2O_4COOH - MWCNT$ gas sensing films were prepared with cleaning of QCM electrode with acetone, ethanol, 2-propanol, purchased from Sigma-Aldrich, and were rinsed for 15 minutes respectively. Subsequent to rinsing, the electrodes were dried with high purity N_2. Then, 3 μl of each solution was coated on QCM electrode surface by drop cast. The thin films were left in vacuum oven for 12 h at 45 ^{0}C to dry.

1.3.5 Chitosan - Acid Functionalized Multiwall Carbon Nanotube/Magnetite Hybrid

(MWCNT)–COOH/Fe_3O_4 − chitosan solutions (0.1 mg/ml) were prepared in 1% acetic acid solution and were stirred at room temperature overnight. Chitosan and (MWCNT)–COOH/Fe_3O_4 gas sensing film were prepared with cleaning of QCM electrode with acetone, ethanol, 2-propanol, purchased from Sigma-Aldrich, and were rinsed for 15 minutes respectively. Subsequent to rinsing, the electrodes were dried with high purity N_2. Then, 3 μl of each solution was coated on QCM electrode surface by drop cast. The thin films were left in vacuum oven for 12 h at 45 °C to dry.

1.4 Gases

Chemical and electronic structures of the gas that is used are given in the following table. We covered the material, which would be helpful for us to explain the interactions between the gas molecules.

Table 1.2 : Chemical and electronic structures of gas molecules used in the study shown.

2.EXPERIMENTAL

2.1 Experimental Procedure

Firstly, chitosan was prepared. Powder contained in 1 gram of chitosan with 15 cc of water and 0.09 gram of acetic acid were stirred for 1 hour at 30 degrees on the magnetic stirrer. Then, the mixture obtained is stirred once again with mixture, whose nanoparticles are $CoFe_2O_4COOH - MWCNT$ and $Fe_3O_4COOH - MWCNT$, and mixtures with 4 % and 2 % by volume were obtained. The final mixtures were stirred for 1 day at room temperature. Then, the dispersion was filtered by a 450 nm filter, and 50 μl each dispersion was then drop-cast onto QCM electrodes via a micro-pipette. The electrodes were held for 1 hour to promote smooth film formation. After evaporation of the dispersant, a thin film on the electrodes was obtained. This thin film coated in above mentioned mixtures were taken to the gas chamber so that gas sorption test would be performed.

Gas metering chamber was prepared for QCM setup. A continuous gas flow was carried out with two non-intervention electrodes in the gas chamber. QCM data were acquired by CH 440B software.

Gas measurements were done under three different flow regimes. These are called as periodic, step and linear measurements. A maximum gas flow rate of 150 sccm was used for each of the gas flow regimes during measurements.
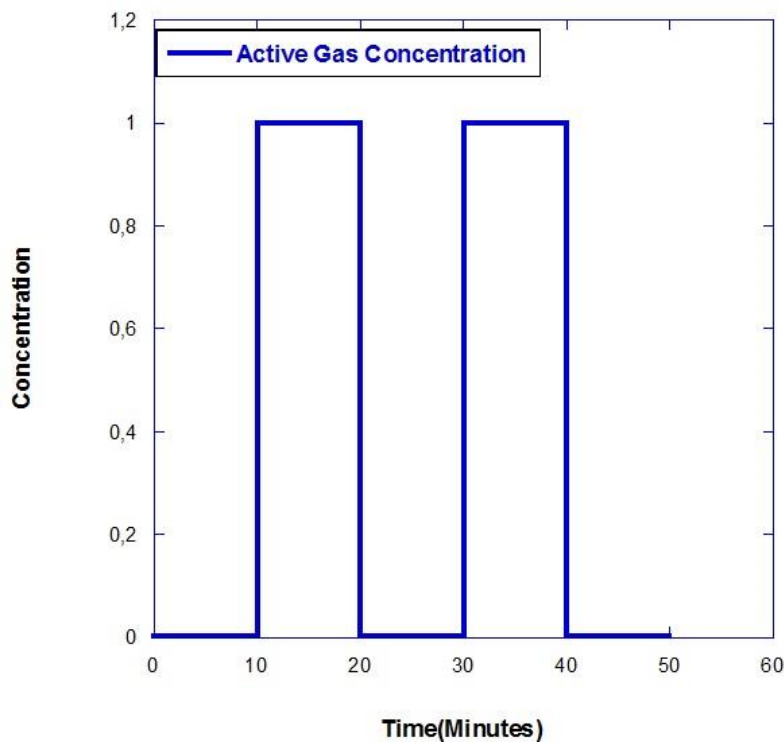
Figure 2.1 Concentration - time graph of periodic gas flow regime.

Figure 2.1 explains how periodic measurements system works. During periodic measurements, first of all, the gas chamber was purged with nitrogen for 600 seconds to remove any gas molecules adsorbed on the chamber and on the thin film-coated electrodes. After that, thin films were exposed to active gases with 100% concentration. This process was repeated twice and aim of that process was to find the reproducibility of gas sensitivity response for each material.

During step measurements, active gas flow concentration was varied from 0% to 100% with 20% increments. Thanks to this method, gas concentration dependent response of each material was assessed.
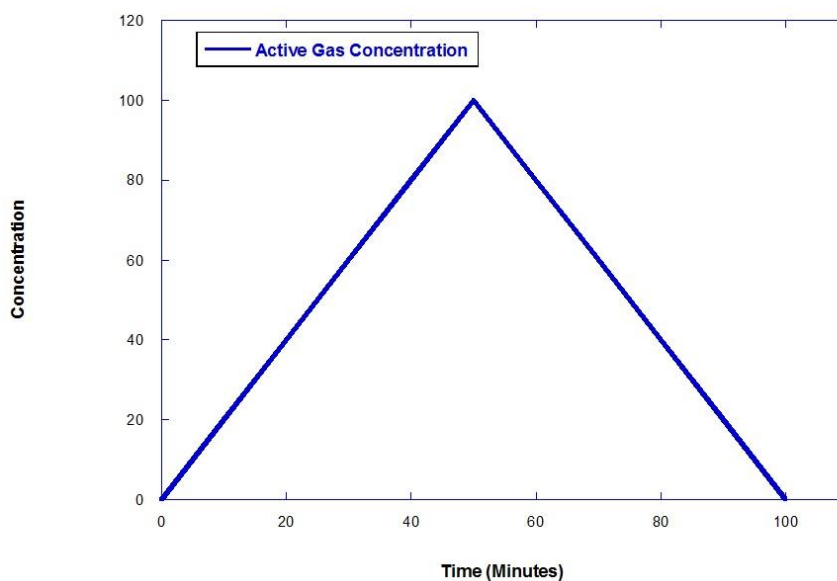
Figure 2.2 Concentration - time graph of linear gas flow regime.

Finally, in linear measurements, active gas flow concentration was varied from 0% to 100% with 4% increments and sensitivity measurements were carried out under this condition.

2.2 Gas Flow Control Measurement System

Gas measurement device can be divided into three parts. First part is gas tubes and mass flow meters connected to a mass flow controller unit. A gas flow set point is regulated on the mass flow controller unit and mass flow meters connected to the mass flow controller maintain a continuous and stable flow into the gas chamber within the set point ranges. Second part is gas chamber. Being a sealed and airtight cell, this chamber accommodates the QCM electrode which is coated with thin films of gas sensitive materials. All this setup is controlled by a computer.
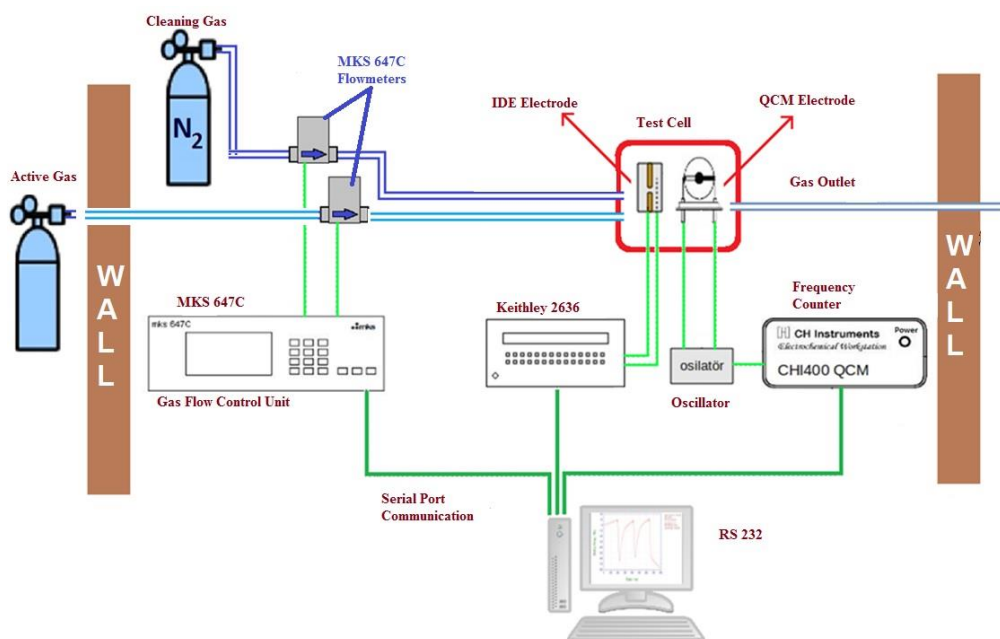
Figure 2.3 : Schematic system of the gas flow control measurement system.

A CHI 400 model electrochemical analyzer (CH Instruments, Austin, US) was used for QCM measurements. The QCM electrodes (International Crystal Manufacturing Co.) had a diameter of 24 mm, density of 2.684 g/cm^3, shear modulus of 2.947 x 1011 g/cm.s^2, circular gold coated areas of 0.196 cm^2 with 6 mm diameter on both sides. CHI400 Series, from CH Instruments (Austin, USA), were used to measure the changes in the resonance frequency of quartz crystals between gold electrodes via both serial and USB interface connected to a computer. The electrodes can oscillate between 7.995 MHz - 7.950 MHz frequency range with a base frequency of 7.995 MHz. The biggest obstruction in these data is that the Sauerbrey equation yields 1.34 ng of adsorbed mass onto the thin film deposited over the gold-coated electrode for 1 Hz of vibrational frequency shift of the QCM electrode.

Six MKS 179A Mass-Flo model mass flow meters (MKS Instruments, US) were used as mass flow meters. Of the six, three had maximum flow rates of 20, 100 and 1000 SCCM (standard cubic centimeter per minute) and were calibrated with CO. The remaining three had maximum flow rates of 100, 1000 and 2000 SCCM and were

calibrated with dry air. With these mass flow meters, gas flow rates as precise as 1 SCCM could easily be achieved. ¼ inch pipes were used to transfer gases from gas tanks to flow meters and from flow meters to the gas chamber. The piping was designed in the following way. The six flow meters in the system were divided into two groups. One was reserved for purging gas nitrogen, and the other five were used for CO, CO_2 and O_2 and other gases. Gas inlets and outlets of the two groups of mass flow meters were joint within each other to achieve mixed gas flows.

Eight-channel model MKS 647C mass flow Controller (MKS instruments, USA) was used to control other six flow meters and the gas flow through the mass. The gas flow to the appliance on / off rates and the designated intervals and remote monitoring real-time flow rate were selected to adjust the flow of gas through the mass flow meter via RS232 interface for PC connection. Also, GCF (gas correction factor) was supported via a parameter with respect to the nitrogen gas calibration.

The results developed through laboratory via MKS 647C and Keithley 2636A, that are real-time the control software, were used within six yards for a purpose, and they developed communication between the resource and mass flow controllers. Concurrent electrical measurement and gas flow control enabled the collection of data through software programs.

Carbon dioxide, oxygen, nitrogen, and ammonia used in the system were 99.9% pure. Diluted with pure N_2 gas 10000 ppm, the gas exits via remote control with commands operated parallel port from a PC, and also electro valves, which organizes the order of carbon monoxide.

Six mass flow meters in a test cell, the surrounding resources, precision measuring devices and Faraday cage of electromagnetic interference in a gas chamber were used to eliminate carbon monoxide leak. Additionally, industrial scientific commercial model M40 CO sensor was used to detect carbon monoxide gas leak as a precaution,

in order to monitor the level of leak in the environment. The whole measurement systems were controlled by using a remote control software, such as team viewer, from a PC.

3. RESULT AND DISCUSSION

In this section, the properties of materials used in gas sensing, quartz crystal micro-technique were examined.

Frequency shift of coated electrodes which was caused by the gas sorption measured by using CHI 400B time-resolved (EQCM) analyzer (distance moved) ought to be measured in order to figure out the gas sensor responses of thin film-coated QCM electrodes.

For each QCM electrode, initial resonance frequency (f_0) values were recorded beforehand for the coating. Following the coating, resonance frequencies for each coated QCM electrode were once again recorded. After that, as stated in Sauerbrey equation, following the thin film deposition, mass of thin film material (Δm_0) which had been deposited on QCM electrode was obtained from the frequency difference.

$$\Delta m = 1.34 ng \; x \; \Delta f_0 \qquad (3.22)$$

After that, we were able to calculate the mass of the gas molecules (Δm) that were adsorbed on the surface of thin film coated electrode after we had put frequency shift (Δf) value of electrode which was caused by the gas sorption into Sauerbrey equation.

$$\Delta m = 1.34 ng \; x \; \Delta f \qquad (3.23)$$

In the end, the ratio between the mass of thin film material that was deposited on QCM electrode per mil and the gas molecules (Δm) which was accumulated on surface of

thin film coated QCM electrode (Δm_0) was determined as the sensor response (S) of each sensor material to CO, CO2 and O2.

$$S = \frac{\Delta m}{\Delta m_0} \ x \ 1000 \qquad\qquad (3.24)$$

The frequency dependent on the sensor response relation was gathered following substituting Δm and Δm_0 with Δf and Δf_0 in the mentioned order.

3.1. Quartz Crystal Microbalance Results

Gas sorption properties of chitosan based nanoparticles against CO, CO_2 and O_2 were analyzed by the QCM technique. Raw data graphics of them can be observed in this part. The sensor responses of those nanoparticles were calculated in accordance with the experimental results.

3.1.2. Periodic measurements results
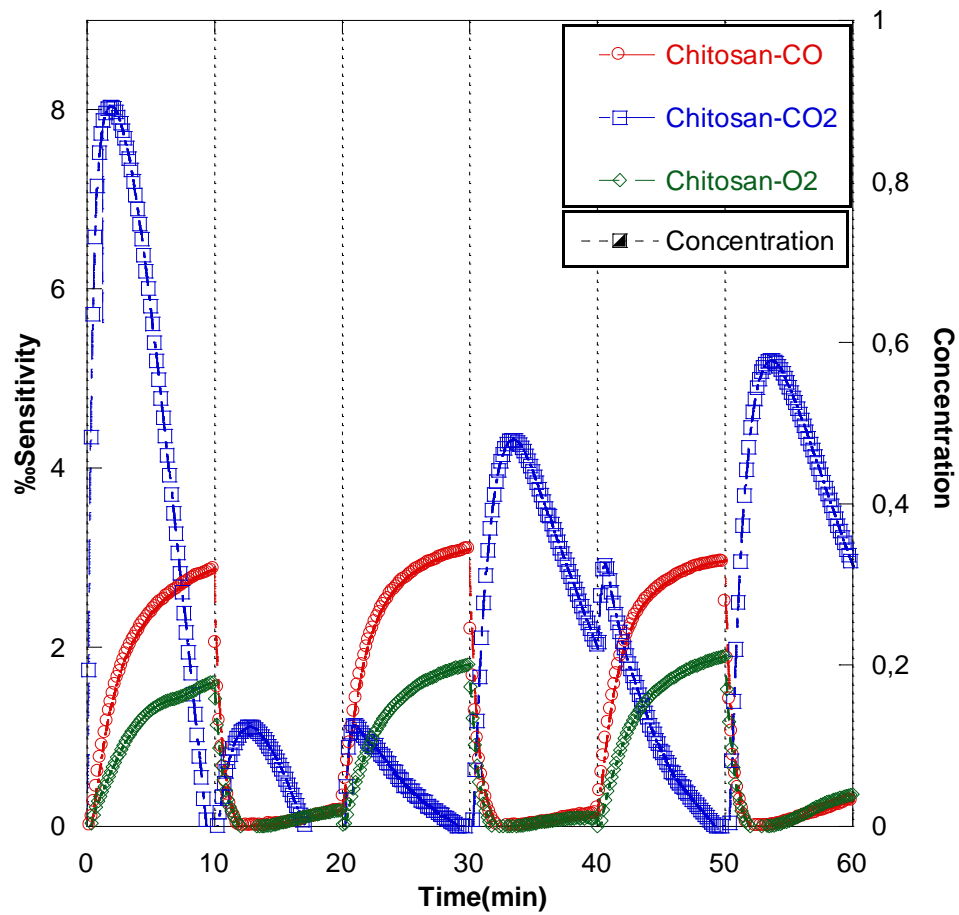
Figure 3.1 demonstrates the responses of chitosan-based thin film to CO, CO_2 and O_2 under the periodic gas flow regime, under N_2 gas environment.

Sensitivity calculations were performed in this part. Since all of the experiments were carried out with the same thin film coated QCM electrode, all gas treatment parameters were the same.

Figure 3.2 demonstrates the responses of chitosan-based $CoFe_2O_4COOH -$

MWCNT 2% thin film to CO, CO_2 and O_2 under the periodic gas flow regime, under

N_2 gas environment.

Sensitivity calculations were performed in this part. Since all of the experiments

were carried out with the same thin film coated QCM electrode, all gas treatment

parameters were the same.

The response time of chitosan based $CoFe_2O_4COOH - MWCNT$ 2%

nanocomposite thin film to gases was short, which means that the film was very

active to gases. The increase in frequency during the first period of 600 seconds

verifies the fact that there still were adsorbed gas molecules on the film, that is, the

film was rather active to the gases. The film was very active because the surface area

increased due to the nanoparticules doping. The film displays higher affinity to O_2

was observed. In a similar way, it was thought that CO. measurements done

previously may have caused higher response against CO_2. O_2 graphics shows that

while the frequency shift was ‰12 at the end of the third desorption period, it was

approximately ‰ 7 at the last part of the second desorption period, which proved that

there still were O_2 molecules on the surface of the film. The porosity of the film could be

the cause of the poor cleaning on the surface. Likewise, when looked at the second cylce,

it can be seen that the adsorbed molecules were partly removed from the surface of the

thin film for all of the gases. When we sort the sensor responses in a descending manner,

the sequence would be as O_2, CO, and CO_2. More affinity O_2 towards was seen because

of the strong hydrogen binding. Nevertheless, the sequence of sensor responses against

other gases was not proportional towards the molar mass of molecules, however, it was

still considered that the above-mentioned assumption may have held true if the period

had been kept shorter, because the response towards CO_2 was decreasing gradually,

which caused the sequence to be spoiled.

Figure 3.3 demonstrates the responses of chitosan-based $CoFe_2O_4COOH$ −

MWCNT 4% thin film to CO, CO_2 and O_2 under the periodic gas flow regime, under

N_2 gas environment.

Sensitivity calculations were performed in this part. Since all of the experiments

were carried out with the same thin film coated QCM electrode, all gas treatment
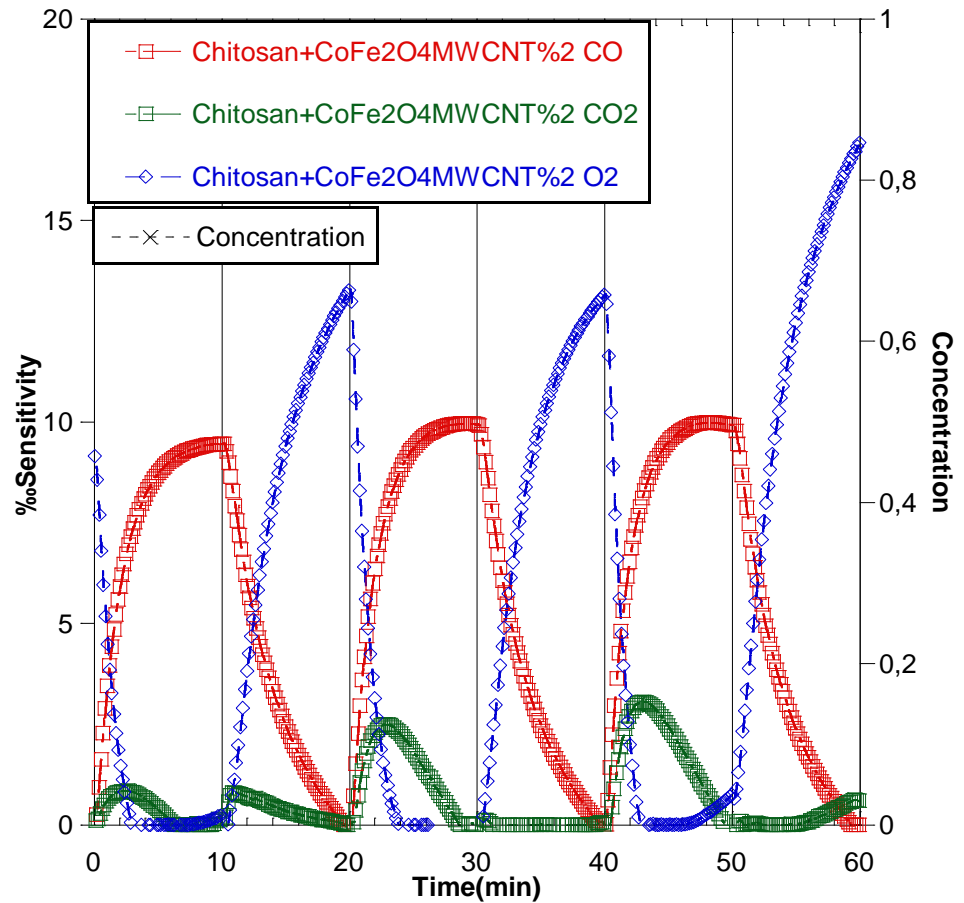
parameters were the same.

The response time of chitosan based $CoFe_2O_4COOH - MWCNT\ 4\%$ nanocomposite thin film to gases was short, which means that the film was very active to gases. The increase in frequency during the first period of 600 seconds verifies the fact that there still were adsorbed gas molecules on the film, that is, the film was rather active to the gases. The film was very active because the surface area increased due to the nanoparticules doping. The film displays higher affinity to O_2 was observed. In a similar way, it was thought that CO. measurements done previously may have caused higher response against CO_2. O_2 graphics shows that while the frequency shift was ‰10 at the end of the second desorption period, it was approximately ‰6 at the last part of the second desorption period, which proved that there still were CO molecules on the surface of the film. The porosity of the film could be the cause of the poor cleaning on the surface. Likewise, when looked at the second cylce, it can be seen that the adsorbed molecules were partly removed from the surface of the thin film for all of the gases. When we sort the sensor responses in a descending manner, the sequence would be as O_2, CO, and CO_2. More affinity O_2 towards was seen because of the strong hydrogen binding. Nevertheless, the sequence of sensor responses against other gases was not proportional towards the molar mass of molecules.

Figure 3.4 demonstrates the responses of chitosan-based $Fe_3O_4COOH -$

MWCNT 2% thin film to CO, CO_2 and O_2 under the periodic gas flow regime, under

N_2 gas environment.

Sensitivity calculations were performed in this part. Since all of the experiments

were carried out with the same thin film coated QCM electrode, all gas treatment

parameters were the same.

The response time of chitosan based $Fe_3O_4COOH - MWCNT$ 2% nanocomposite thin film to gases was short, which means that the film was very active to gases. The increase in frequency during the first period of 600 seconds verifies the fact that there still were adsorbed gas molecules on the film, that is, the film was rather active to the gases. The film was very active because the surface area increased due to the nanoparticules doping. The film displays higher affinity to CO. CO graphics shows that while the frequency shift was ‰7 at the end of the first desorption period, it was approximately ‰10 at the last part of the second desorption period, which proved that there still were CO molecules on the surface of the film. The porosity of the film could be the cause of the poor cleaning on the surface. Likewise, when looked at the second cylce, it can be seen that the adsorbed molecules were partly removed from the surface of the thin film for all of the gases. When we sort the sensor responses in a descending manner, the sequence would be as CO, O_2 and CO_2. Nevertheless, the sequence of sensor responses against other gases was not proportional towards the molar mass of molecules, however, it was still considered that the above-mentioned assumption may have held true if the period had been kept shorter, because the response towards CO_2 was decreasing gradually, which caused the sequence to be spoiled.
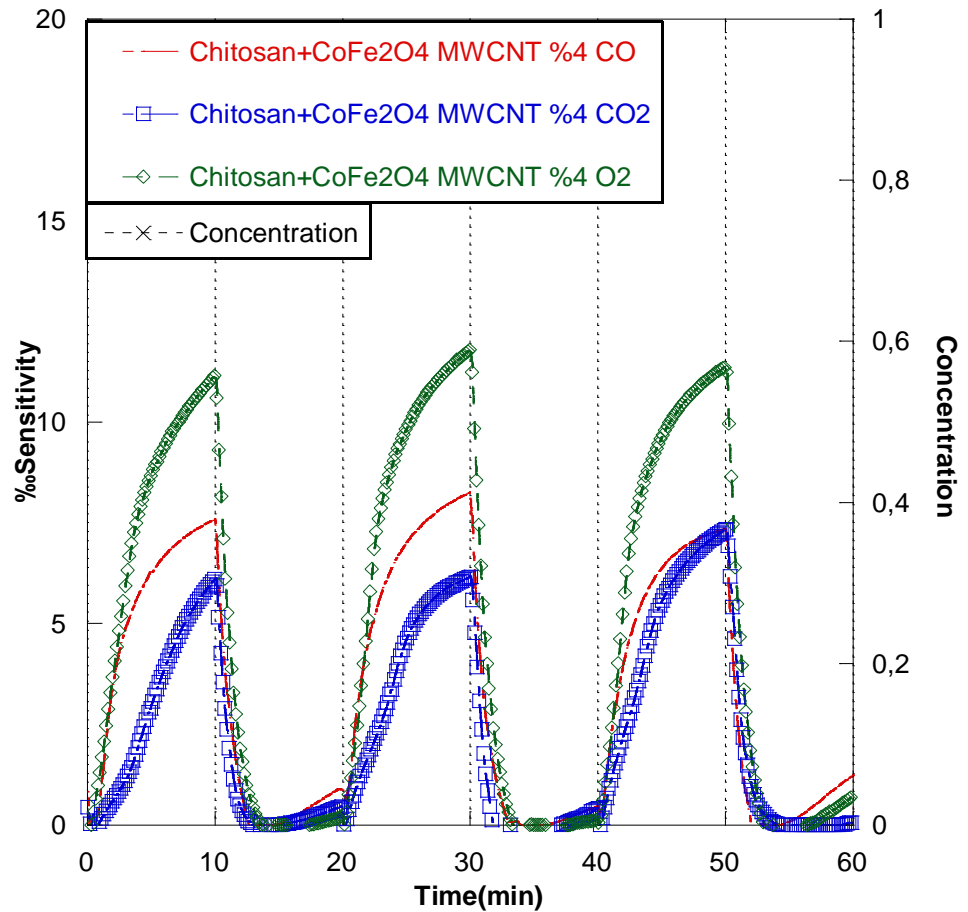
Figure 3.5 demonstrates the responses of chitosan-based $Fe_3O_4COOH -$

MWCNT 4% thin film to CO, CO_2 and O_2 under the periodic gas flow regime, under

N_2 gas environment.

Sensitivity calculations were performed in this part. Since all of the experiments

were carried out with the same thin film coated QCM electrode, all gas treatment

parameters were the same.

The response time of chitosan based $Fe_3O_4COOH - MWCNT$ 4% nanocomposite thin film to gases was short, which means that the film was very active to gases. The increase in frequency during the first period of 600 seconds verifies the fact that there still were adsorbed gas molecules on the film, that is, the film was rather active to the gases. The film was very active because the surface area increased due to the nanoparticules doping. The film displays higher affinity to CO. graphics shows that while the frequency shift was ‰6 at the end of the first desorption period, it was approximately ‰7 at the last part of the second desorption period, which proved that there still were CO molecules on the surface of the film. The porosity of the film could be the cause of the poor cleaning on the surface. Likewise, when looked at the second cylce, it can be seen that the adsorbed molecules were partly removed from the surface of the thin film for all of the gases. When we sort the sensor responses in a descending manner, the sequence would be as CO, O_2 and CO_2. Nevertheless, the sequence of sensor responses against other gases was not proportional towards the molar mass of molecules, however, it was still c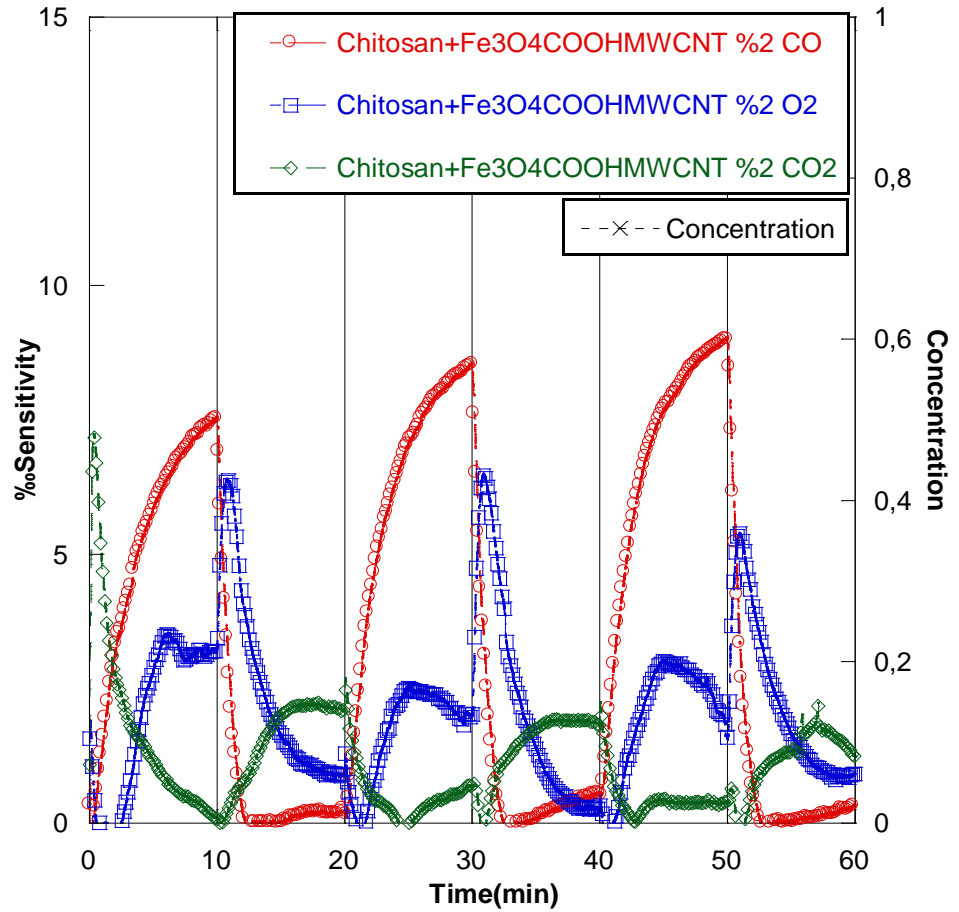onsidered that the above-mentioned assumption may have held true if the period had been kept shorter, because the response towards CO_2 was decreasing gradually, which caused the sequence to be spoiled.

Figure 3.6 demonstrates the responses of chitosan-based thin film to CO, CO_2 and

O_2 under the periodic gas flow regime, under air environment.

Sensitivity calculations were performed in this part. Since all of the experiments

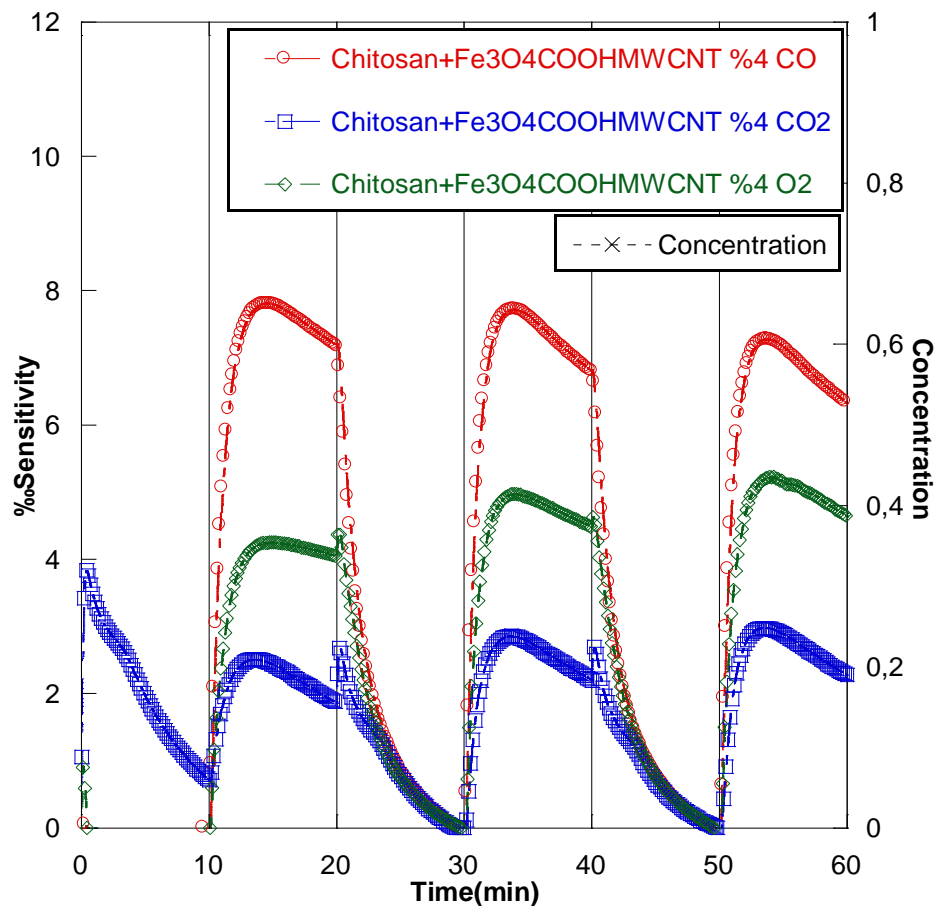were carried out with the same thin film coated QCM electrode, all gas treatment

parameters were the same.

Figure 3.7 demonstrates the responses of chitosan-based $CoFe_2O_4COOH-$

MWCNT 2% thin film to CO, CO_2 and O_2 under the periodic gas flow regime, under

air environment.

Sensitivity calculations were performed in this part. Since all of the experiments

were carried out with the same thin film coated QCM electrode, all gas treatment

parameters were the same.

The response time of chitosan based $CoFe_2O_4COOH - MWCNT$ 2% nanocomposite thin film to gases was short, which means that the film was very active to gases. The increase in frequency during the first period of 600 seconds verifies the fact that there still were adsorbed gas molecules on the film, that is, the film was rather active to the gases. The film was very active because the surface area increased due to the nanoparticules doping. The film displays higher affinity to O_2 was observed. In a similar way, it was thought that CO. measurements done previously may have caused higher response against CO_2. O_2 graphics shows that while the frequency shift was ‰30 at the end of the first desorption period, it was approximately ‰ 15 at the last part of the second desorption period, which proved that there still were O_2 molecules on the surface of the film. The porosity of the film could be the cause of the poor cleaning on the surface. Likewise, when looked at the second cylce, it can be seen that the adsorbed molecules were partly removed from the surface of the thin film for all of the gases. When we sort the sensor responses in a descending manner, the sequence would be as O_2, CO, and CO_2. More affinity O_2 towards was seen because of the strong hydrogen binding. Nevertheless, the sequence of sensor responses against other gases was not proportional towards the molar mass of molecules, however, it was still considered that the above-mentioned assumption may have held true if the period had been kept shorter, because the response towards CO_2 was decreasing gradually, which caused the sequence to be spoiled.
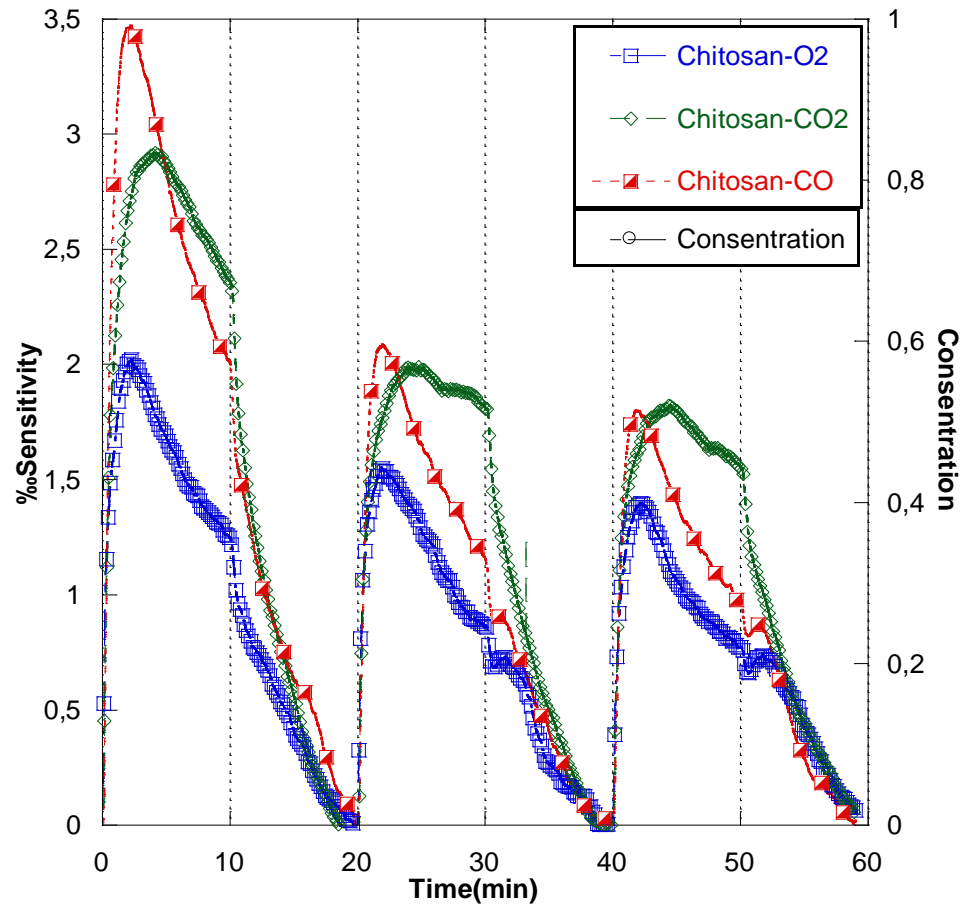
Figure 3.8 demonstrates the responses of chitosan-based $CoFe_2O_4COOH -$

MWCNT 4% thin film to CO, CO_2 and O_2 under the periodic gas flow regime,

under air environment.

Sensitivity calculations were performed in this part. Since all of the experiments

were carried out with the same thin film coated QCM electrode, all gas treatment
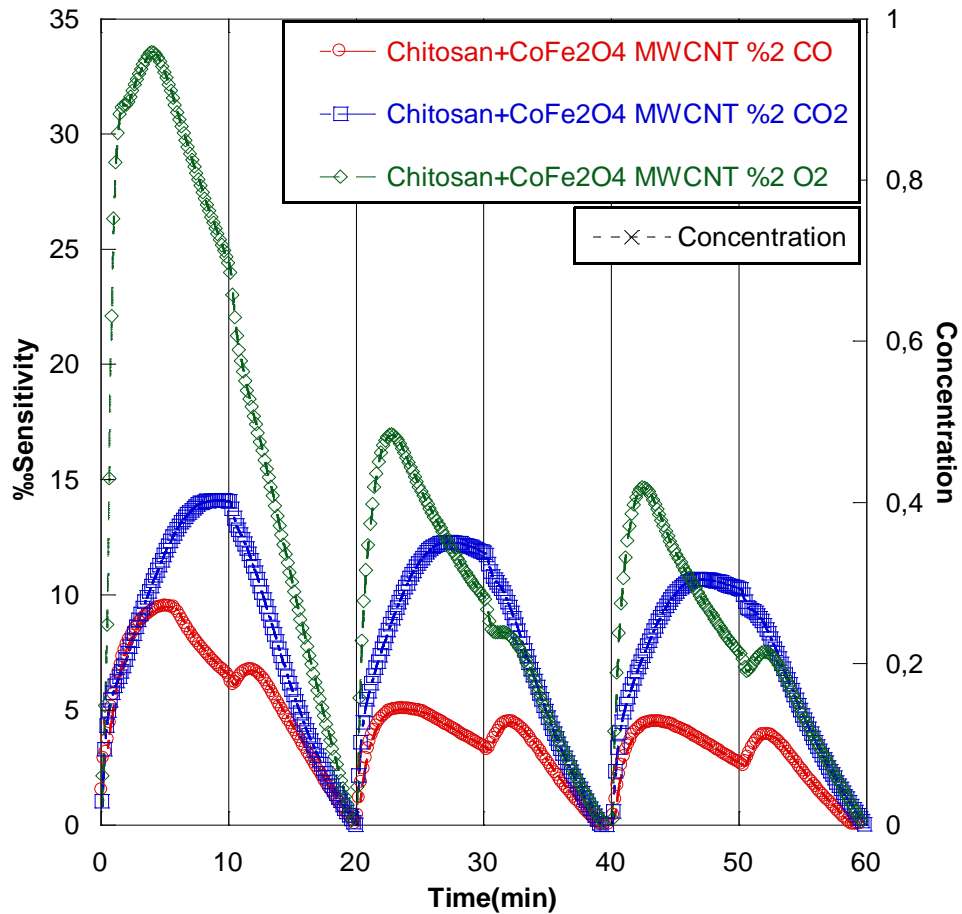
parameters were the same.

The response time of chitosan based $CoFe_2O_4COOH-MWCNT$ 4% nanocomposite thin film to gases was short, which means that the film was very active to gases. The increase in frequency during the first period of 600 seconds verifies the fact that there still were adsorbed gas molecules on the film, that is, the film was rather active to the gases. The film was very active because the surface area increased due to the nanoparticules doping. The film displays higher affinity to CO was observed. In a similar way, it was thought that O_2. measurements done previously may have caused higher response against CO_2. O_2 graphics shows that while the frequency shift was ‰10 at the end of the second desorption period, it was approximately ‰6 at the last part of the second desorption period, which proved that there still were CO molecules on the surface of the film. The porosity of the film could be the cause of the poor cleaning on the surface. Likewise, when looked at the second cylce, it can be seen that the adsorbed molecules were partly removed from the surface of the thin film for all of the gases. When we sort the sensor responses in a descending manner, the sequence would be as O_2, CO, and CO_2. More affinity O_2 towards was seen because of the strong hydrogen binding. Nevertheless, the sequence of sensor responses against other gases was not proportional towards the molar mass of molecules.

Figure 3.9 demonstrates the responses of chitosan-based Fe_3O_4COOH −

MWCNT 2% thin film to CO,CO_2 and O_2 under the periodic gas flow regime, under

N_2 gas environment.

Sensitivity calculations were performed in this part. Since all of the experiments

were carried out with the same thin film coated QCM electrode, all gas treatment

parameters were the same.

The response time of chitosan based $Fe_3O_4COOH - MWCNT$ 2% nanocomposite thin film to gases was short, which means that the film was very active to gases. The increase in frequency during the first period of 600 seconds verifies the fact that there still were adsorbed gas molecules on the film, that is, the film was rather active to the gases. The film was very active because the surface area increased due to the nanoparticules doping. The film displays higher affinity to CO. graphics shows that while the frequency shift was ‰45 at the end of the first desorption period, it was approximately ‰25 at the last part of the second desorption period, which proved that there still were CO molecules on the surface of the film. The porosity of the film could be the cause of the poor cleaning on the surface. Likewise, when looked at the second cylce, it can be seen that the adsorbed molecules were partly removed from the surface of the thin film for all of the gases. When we sort the sensor responses in a descending manner, the sequence would be as CO, O_2 and CO_2. Nevertheless, the sequence of sensor responses against other gases was not proportional towards the molar mass of molecules, however, it was still considered that the above-mentioned assumption may have held true if the period had been kept shorter, because the response towards CO_2 was decreasing gradually, which caused the sequence to be spoiled.
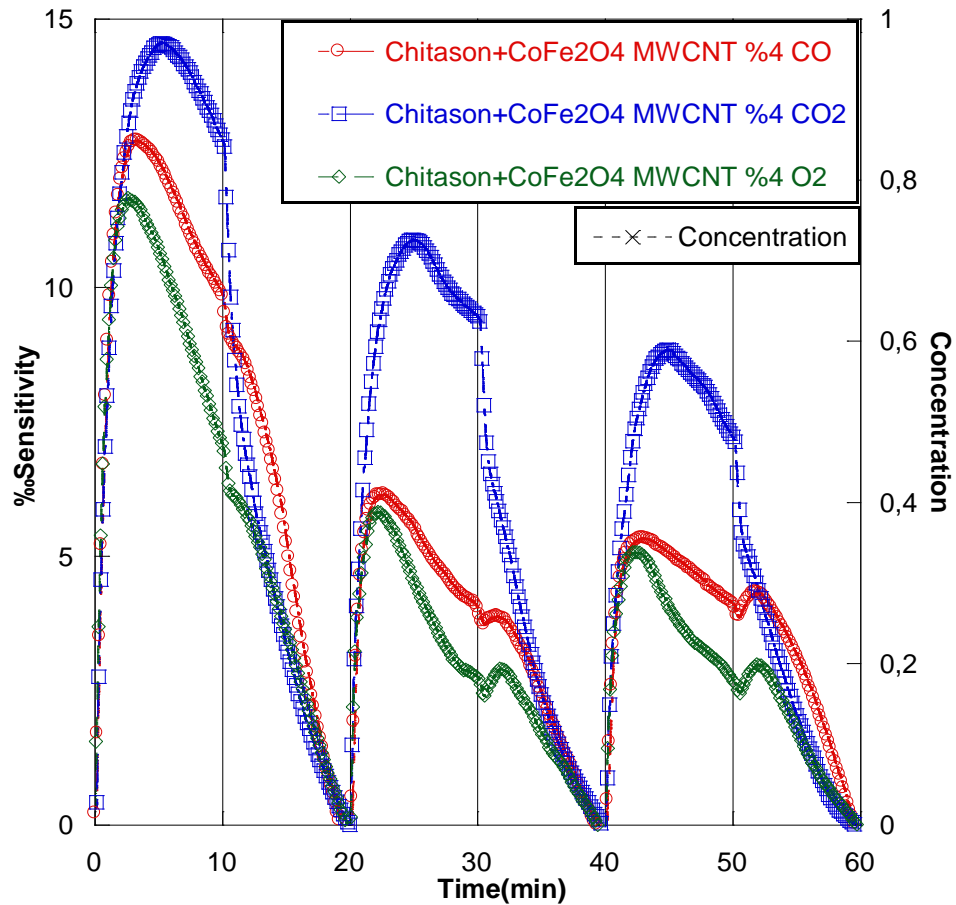
Figure 3.10 demonstrates the responses of chitosan-based $Fe_3O_4COOH -$

MWCNT 4% thin film to CO, CO_2 and O_2 under the periodic gas flow regime, under

air environment.

Sensitivity calculations were performed in this part. Since all of the experiments

were carried out with the same thin film coated QCM electrode, all gas treatment

parameters were the same.

The response time of chitosan based $Fe_3O_4COOH - MWCNT$ 4% nanocomposite thin film to gases was short, which means that the film was very active to gases. The increase in frequency during the first period of 600 seconds verifies the fact that there still were adsorbed gas molecules on the film, that is, the film was rather active to the gases. The film was very active because the surface area increased due to the nanoparticules doping. The film displays higher affinity to CO. graphics shows that while the frequency shift was ‰8 at the end of the first desorption period, it was approximately ‰7 at the last part of the second desorption period, which proved that there still were CO molecules on the surface of the film. The porosity of the film could be the cause of the poor cleaning on the surface. Likewise, when looked at the second cylce, it can be seen that the adsorbed molecules were partly removed from the surface of the thin film for all of the gases. When we sort the sensor responses in a descending manner, the sequence would be as CO, O_2 and CO_2. Nevertheless, the sequence of sensor responses against other gases was not proportional towards the molar mass of molecules, however, it was still c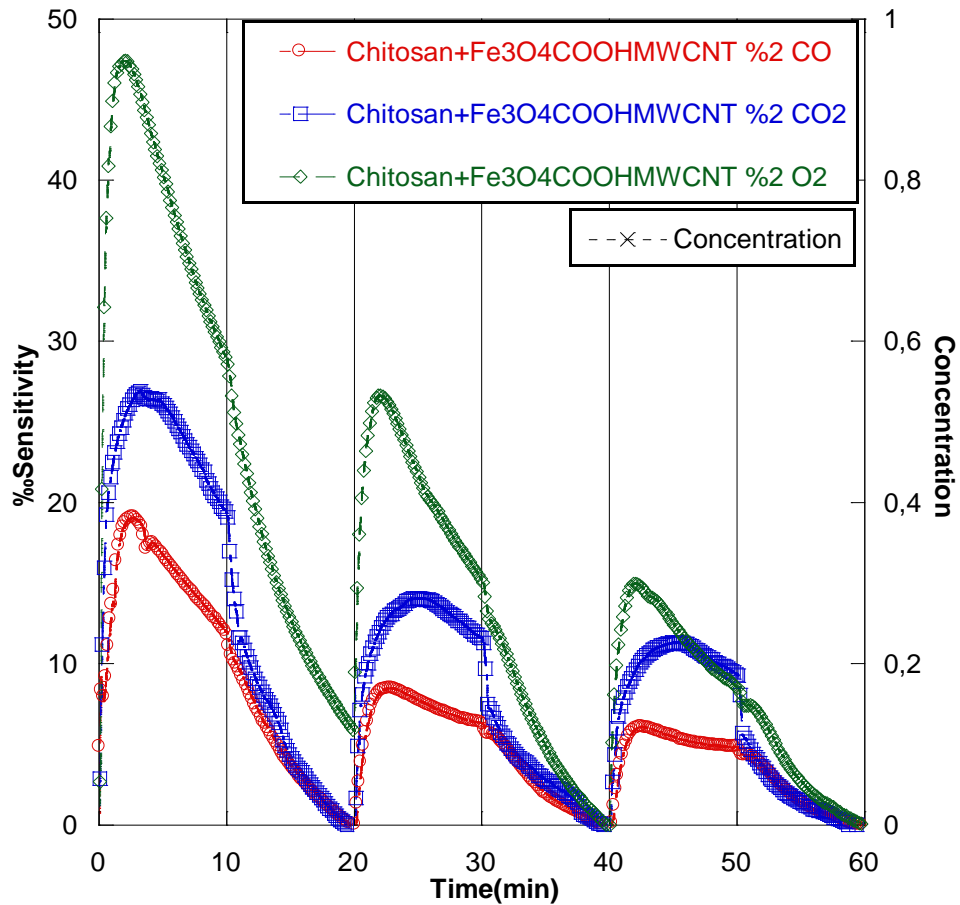onsidered that the above-mentioned assumption may have held true if the period had been kept shorter, because the response towards CO_2 was decreasing gradually, which caused the sequence to be spoiled.
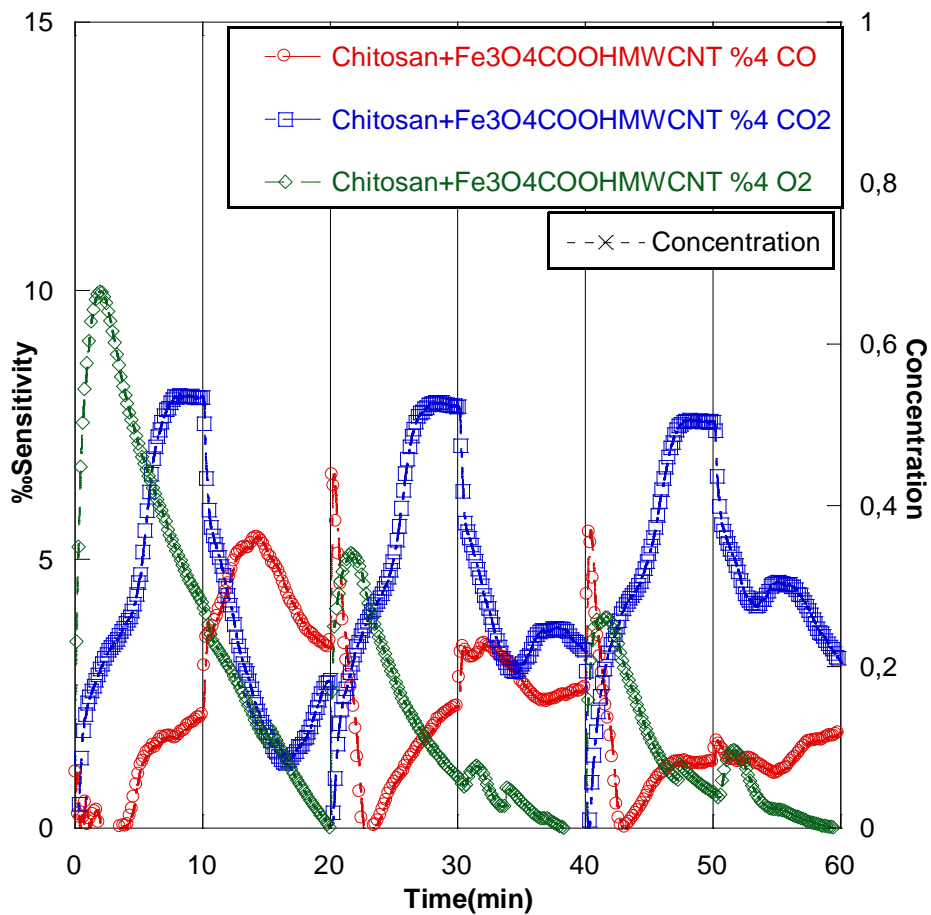
Table 3.1: Maximum sensor response values of all conducted materials, under N_2 gas environment.

Materials	Maximum sensor response value (‰)		
	CO	CO_2	O_2
Chitosan	2.96	8.13	1.89
Chitosan $+ CoFe_2O_4COOH - MWCNT \%2$	10.05	3.00	13.33
Chitosan $+ CoFe_2O_4COOH - MWCNT \%4$	8.13	7.36	11.75
Chitosan $+ Fe_3O_4COOH - MWCNT\%2$	9.08	7.13	6.55
Chitosan $+ Fe_3O_4COOH - MWCNT\%4$	7.82	3.86	5.22

Table 3.2: Maximum sensor response values of all conducted materials, under air environment.

Materials	Maximum sensor response value (‰)		
	CO	CO_2	O_2
Chitosan	3.48	2.92	2.03
Chitosan $+ CoFe_2O_4COOH - MWCNT\ \%2$	9.72	14.48	33.63
Chitosan $+ CoFe_2O_4COOH - MWCNT\ \%4$	12.79	14.70	11.50
Chitosan $+ Fe_3O_4COOH - MWCNT\%2$	18.88	27.22	47.50
Chitosan $+ Fe_3O_4COOH - MWCNT\%4$	6.61	8.12	9.96

In order to eliminate the effect of the mass of the film coated on QCM electrode, an optimization was applied. The final result was calculated as the sensor response mentioned above. The F_0 value is defined as the frequency shift between the coated and the uncoated QCM electrode.

Because of the fact that that value must not exceed the working range of QCM electrode, the mass of coated film is essential. For this reason, the property of the thin film is pertinent to the molar mass of used material. The most essential property of the gas used for gas adsorption process is the fact that molecules have active sites that have an impact on the interaction in between the thin film and the active gas. Those bindings in between active sites and the adsorption gases contain Van der Waals interaction or hydrogen bonding. It can be inferred that the amount of active sites are fairly important for the adsorption process.

The sensor responses were optimized in accordance with the calculation stated above; yet, the changes on the surface area and porosity because of the $CoFe_2O_4COOH - MWCNT$ and $Fe_3O_4COOH - MWCNT$ doping and chitosan conjugation were not taken into consideration. But the most important part was that the parameters that are in direct relation with the sensor response, such as the changes in the mass of the thin film by conjugation or doping and the correlation between the amount of active sites as a result of doping conjugation were not observed at the first sight. There is not supposed to be any changes in the amount of active sites if it considered as monomer, however the surface area might have increased. Besides this, the mass of prepared nanocomposite film will have been increased because the molecular weight of the $Fe_3O_4COOH - MWCNT$ is 276.5500 g/mol, while the molar mass of $CoFe_2O_4COOH - MWCNT$ is 279.6382 g/mol.

The sensor response of chitosan against CO_2 8.13‰ on the other hand

$CoFe_2O_4COOH - MWCNT\ 2\%$ is 3.00‰, and it is 7,36‰ under N_2 gas environment

for $CoFe_2O_4COOH - MWCNT\ 4\%$ nanocomposite.

The sensor response of chitosan against CO_2 3,48‰ on the other hand

$Fe_3O_4COOH - MWCNT2\%$ is 7.13‰ and it is 3.86‰ under N_2 gas environment for

$Fe_3O_4COOH - MWCNT4\%$ nanocomposite. It seems best solution mixes is vol 2%.

The sensor response of chitosan against CO_2 2.92‰ on the other hand

$CoFe_2O_4COOH - MWCNT\ 2\%$ is 14.48‰, and it is 14.70‰ under air environment

for $CoFe_2O_4COOH - MWCNT\ 4\%$ nanocomposite.

The sensor response of chitosan against CO_2 3,48‰ on the other hand

$Fe_3O_4COOH - MWCNT2\%$ is 27.22‰ and it is 8.12‰ under air environment for

$Fe_3O_4COOH - MWCNT4\%$ nanocomposite. It seems best solution mixes is vol 2%.

The sensor response of chitosan against CO **3.48‰** on the other hand $CoFe_2O_4COOH -$

$MWCNT\ 2\%$ is 10.05‰, and it is 8.13‰ under N_2 gas environment for

$CoFe_2O_4COOH - MWCNT\ 4\%$ nanocomposite. It seems best solution mixes is vol

2%.

The sensor response of chitosan against CO 2.96‰ on the other hand

$Fe_3O_4COOH - MWCNT2\%$ is 9.08‰ and it is 7.82‰ under N_2 gas environment for

$Fe_3O_4COOH - MWCNT4\%$ nanocomposite. It seems best solution mixes is vol 2%.

The sensor response of chitosan against CO 3.48‰ on the other hand $CoFe_2O_4COOH -$

$MWCNT\ 2\%$ is 9.72‰, and it is 12.79‰ under air environment for $CoFe_2O_4COOH -$

$MWCNT\ 4\%$ nanocomposite.

The sensor response of chitosan against CO 3.48‰ on the other hand

$Fe_3O_4COOH - MWCNT2\%$ is 18.88‰ and it is 6.61‰ under air environment for

$Fe_3O_4COOH - MWCNT4\%$nanocomposite. It seems best solution mixes is vol 2%.

The sensor response of chitosan against O_2 1.89‰ on the other hand $CoFe_2O_4COOH - MWCNT\ 2\%$ is 13.33‰, and it is 11.75‰ under N_2 gas environment for $CoFe_2O_4COOH - MWCNT\ 4\%$ nanocomposite.

The sensor response of chitosan against O_2 1.89‰ on the other hand $Fe_3O_4COOH - MWCNT2\%$ is 6.55‰ and it is 5.22‰ under N_2 gas environment for $Fe_3O_4COOH - MWCNT4\%$ nanocomposite. It seems best solution mixes is vol 2%.

The sensor response of chitosan against O_2 2.03 on the other hand $CoFe_2O_4COOH - MWCNT\ 2\%$ is 33.63‰, and it is 11.50‰ under air environment for $CoFe_2O_4COOH - MWCNT\ \%4$ nanocomposite. It seems best solution mixes is vol 2%.

The sensor response of chitosan against O_2 12.03‰ on the other hand $Fe_3O_4COOH - MWCNT2\%$ is 47.50‰ and it is 9.96‰ under air environment for $Fe_3O_4COOH - MWCNT4\%$ nanocomposite. It seems best solution mixes is vol 2%.

3.1.2. Lineer measurements results

Figure 3.11 demonstrates the responses of chitosan-based   thin film to CO,CO_2 and

O_2 under the linear gas flow regime, under N_2 gas environment.

Response of chitosan based films are vastly linear and have reversible character but

CO and O_2 gases, non-linear effect is observed.

Figure 3.12 demonstrates the responses of chitosan-based $CoFe_2O_4COOH-$ MWCNT 2% thin film to CO, CO_2 and O_2 under the linear gas flow regime, under N_2 gas environment.

Figure 3.13 demonstrates the responses of chitosan-based $CoFe_2O_4COOH-$

MWCNT 4% thin film to CO,CO_2 and O_2 under the linear gas flow regime, under

N_2 gas environment.

Figure 3.14 demonstrates the responses of chitosan-based $Fe_3O_4COOH -$

MWCNT 2% thin film to CO, CO_2 and O_2 under the linear gas flow regime, under

N_2 gas environment.

Figure 3.15 demonstrates the responses of chitosan-based $Fe_3O_4COOH -$

MWCNT 4% thin film to CO, CO_2 and O_2 under the linear gas flow regime, under
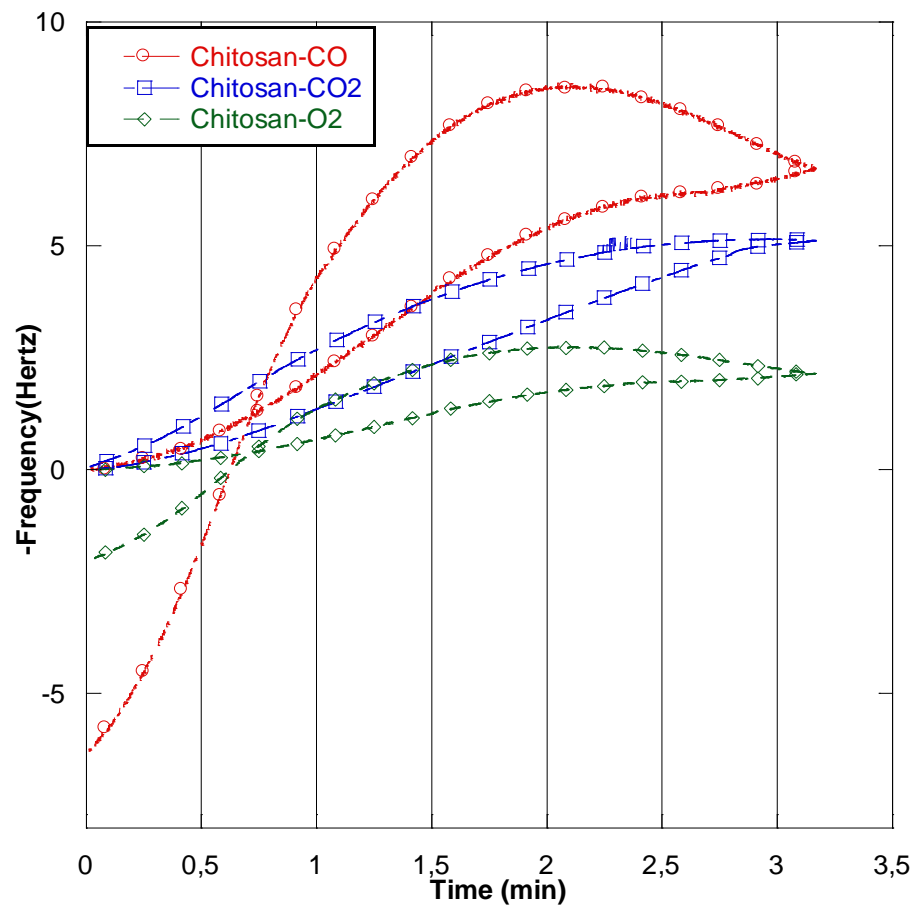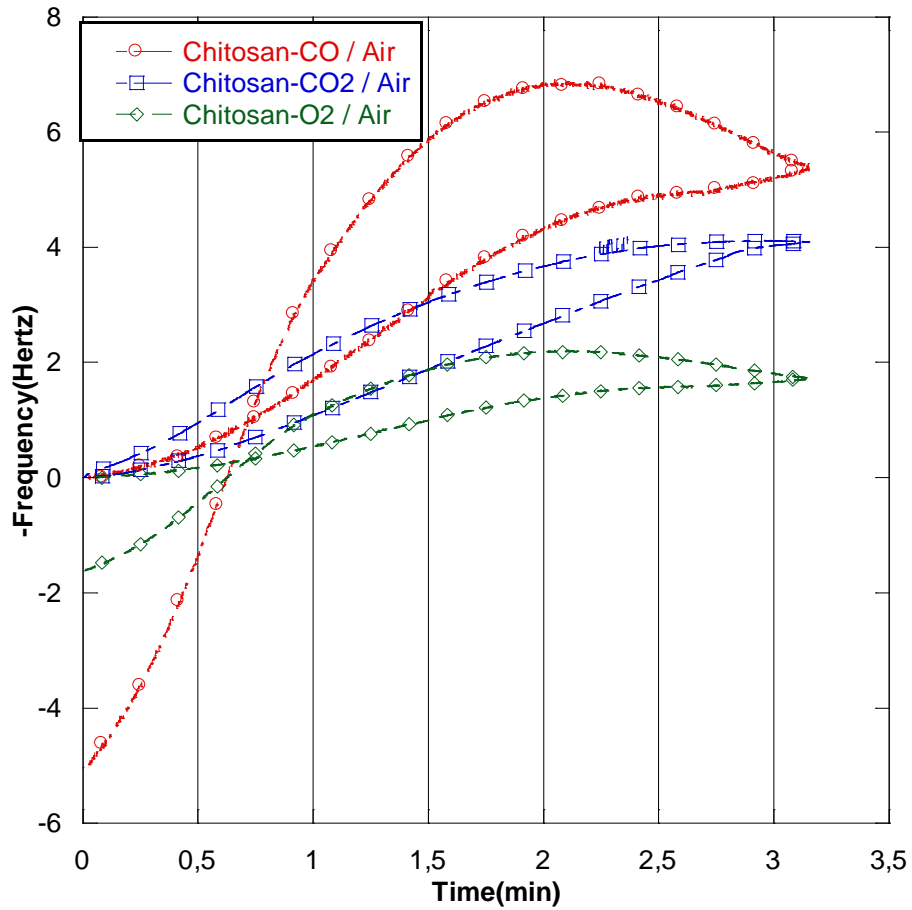
N_2 gas environment.

Figure 3.16 demonstrates the responses of chitosan-based   thin film to CO,CO_2 and

O_2 under the linear gas flow regime, under air environment.

Response of Chitosan based films are vastly linear and have reversible character but

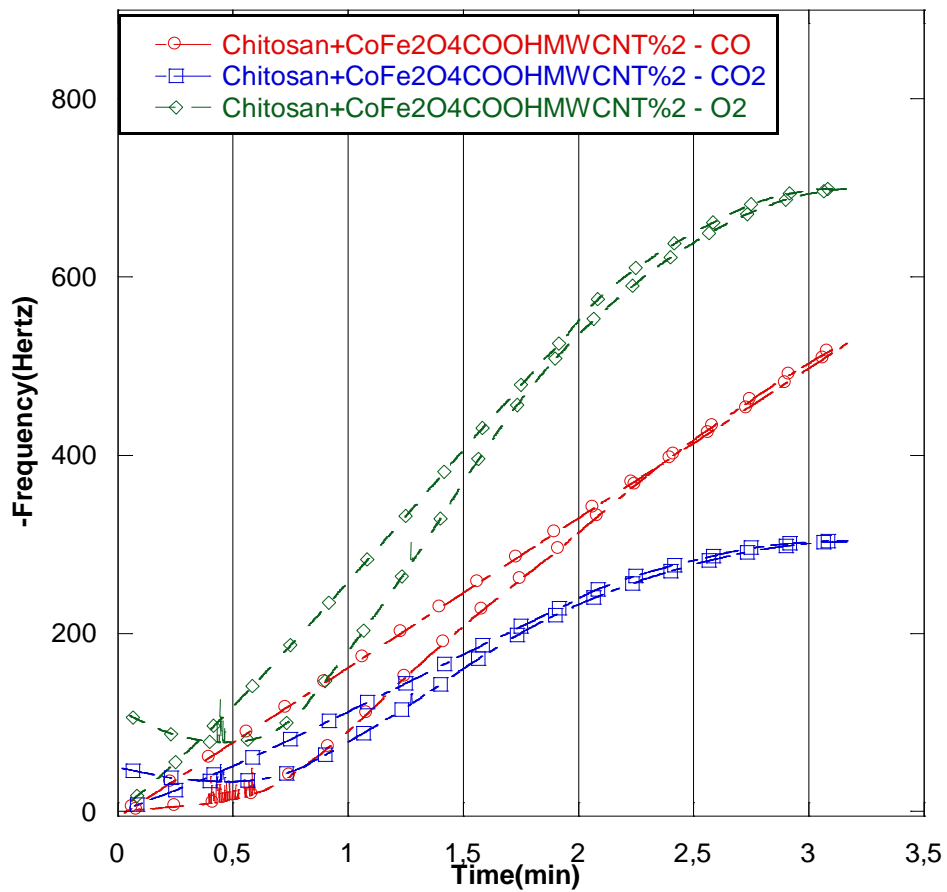CO and O_2 gases, non-linear effect is observed.
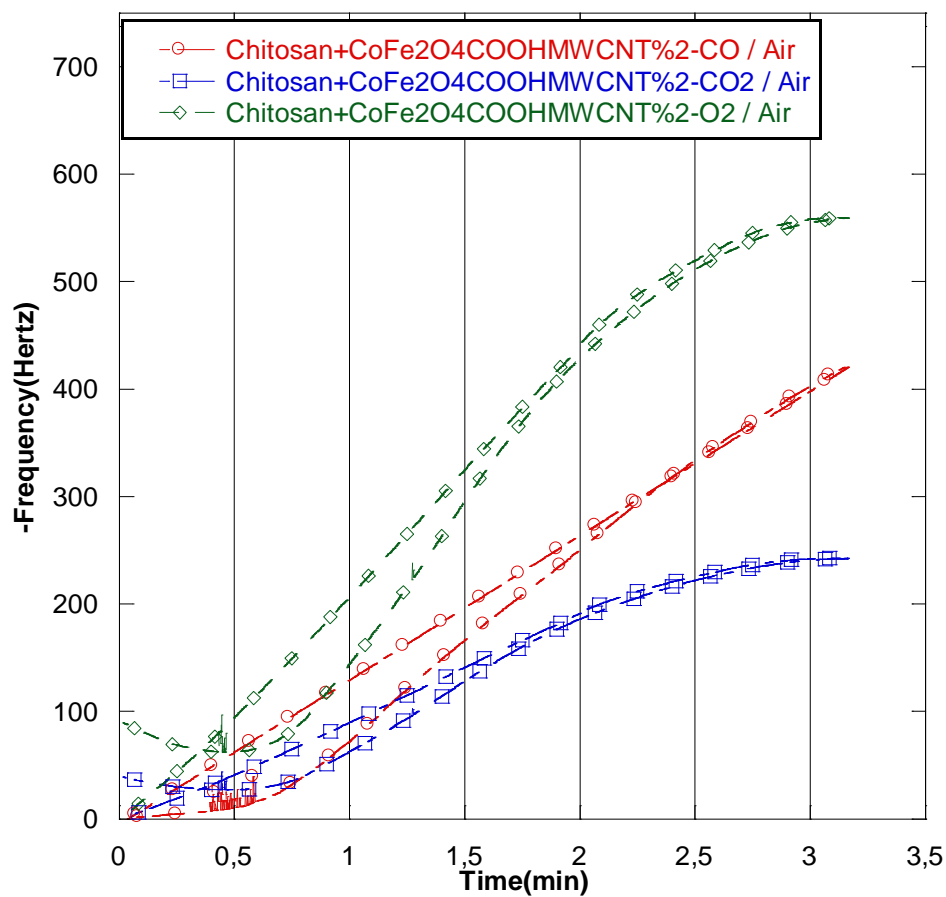
Figure 3.17 demonstrates the responses of chitosan-based $CoFe_2O_4COOH -$ MWCNT 2% thin film to CO, CO_2 and O_2 under the linear gas flow regime, under air environment.
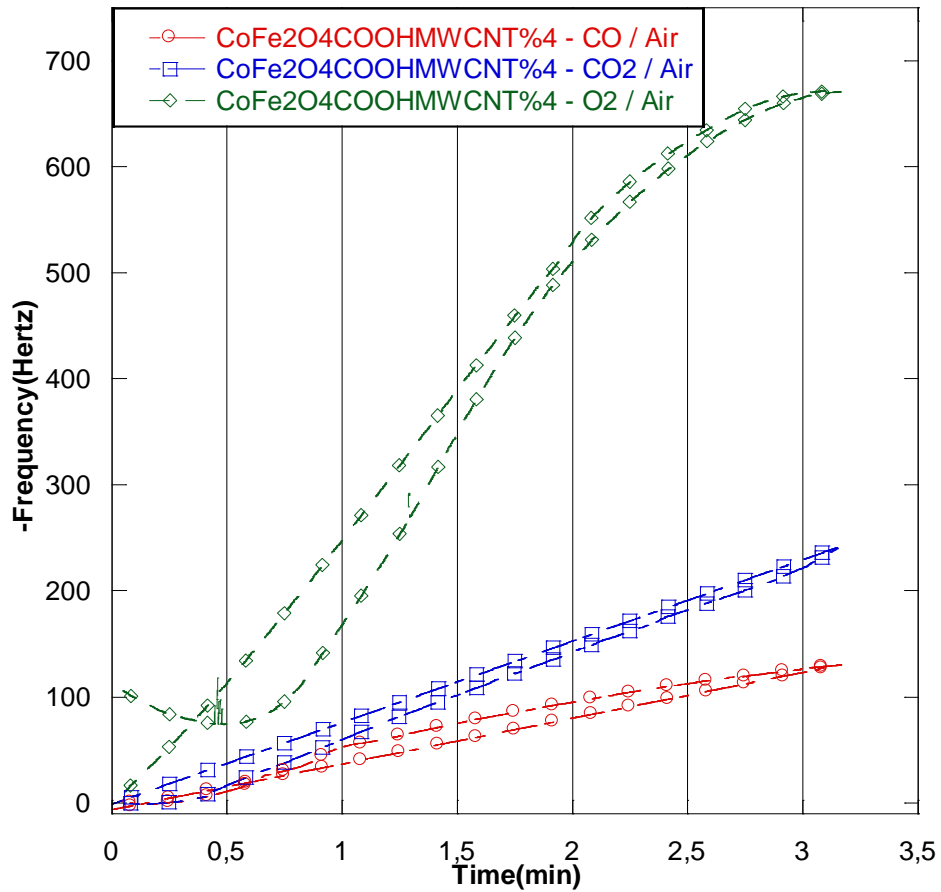
Figure 3.18 demonstrates the responses of chitosan-based $CoFe_2O_4COOH-$

MWCNT 4% thin film to CO, CO_2 and O_2 under the linear gas flow regime, under

air environment.

Figure 3.19 demonstrates the responses of chitosan-based $Fe_3O_4COOH -$ MWCNT 2% thin film to CO, CO_2 and O_2 under the linear gas flow regime, under air environment.
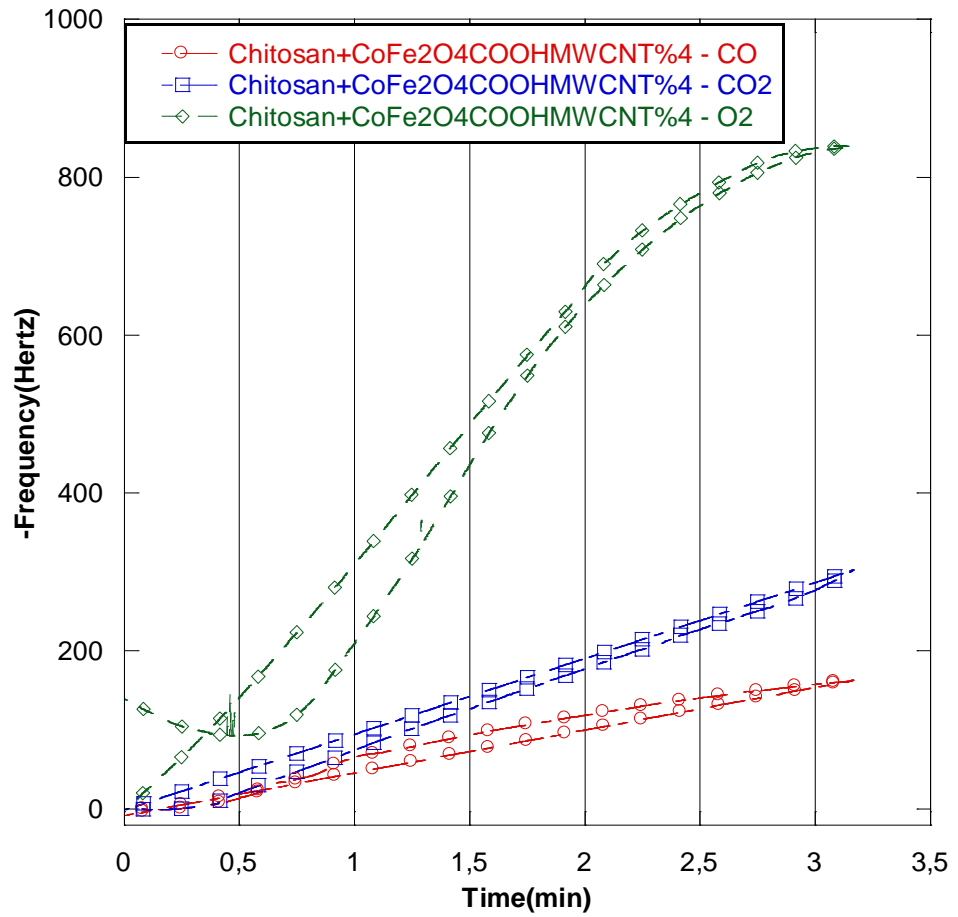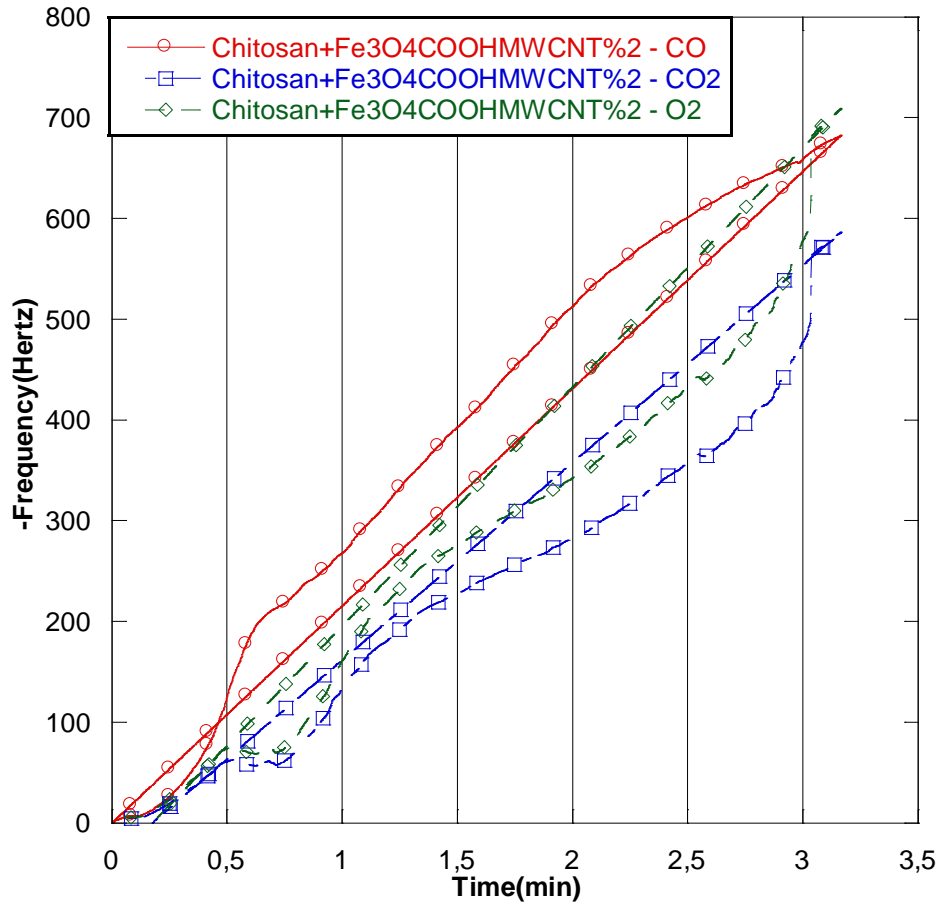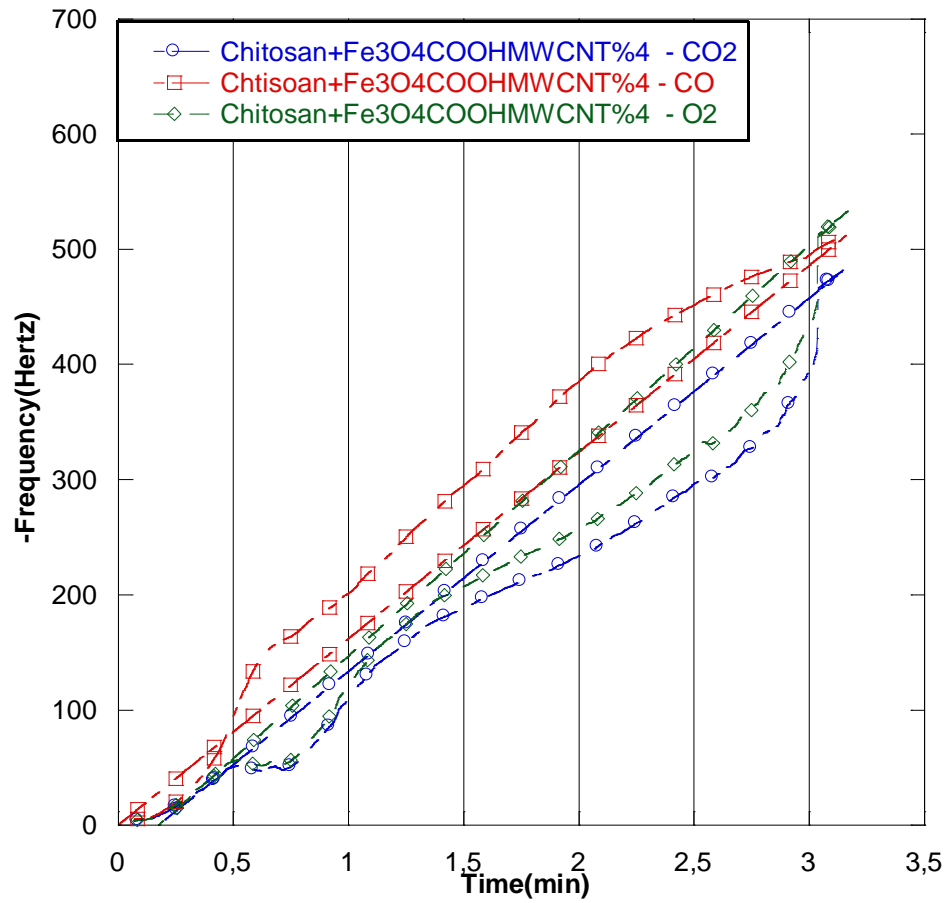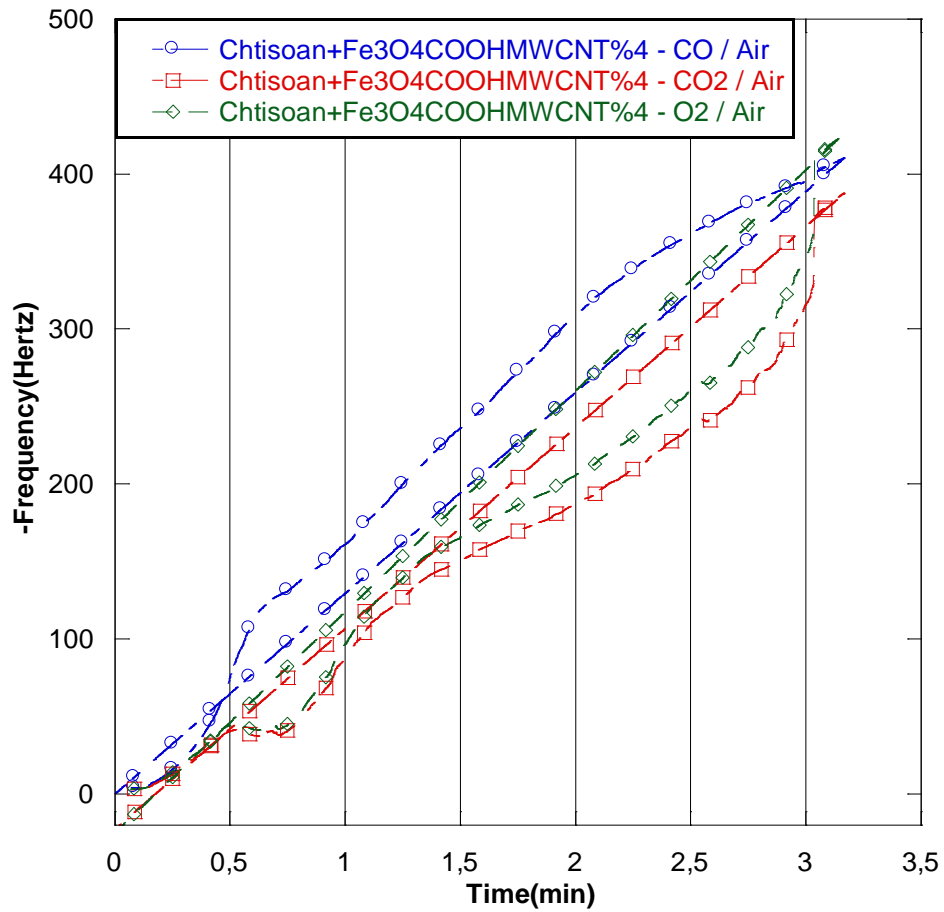
Figure 3.20 demonstrates the responses of chitosan-based Fe_3O_4COOH-
MWCNT 4% thin film to CO, CO_2 and O_2 under the linear gas flow regime, under
air environment.

4. CONCLUSION

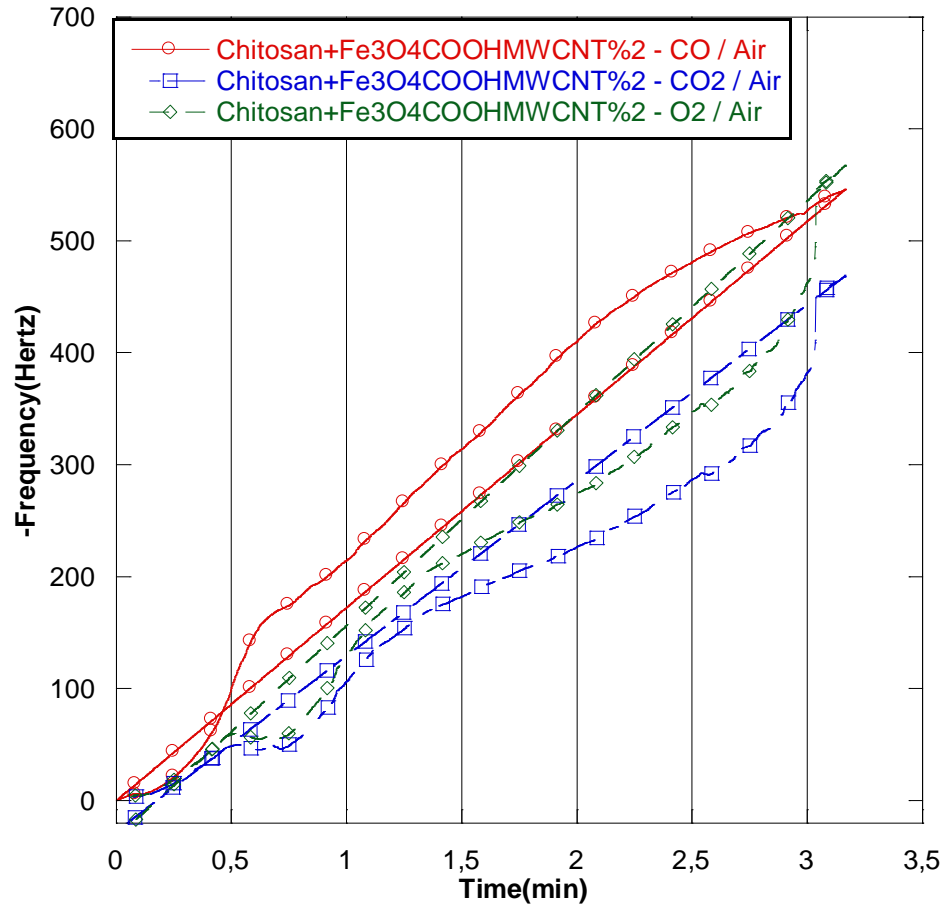The effect of the nanoparticles doping on gas sensing properties of chitosan-based non-conductive polymers was investigated via the quartz crystal microbalance. The sensor responses of chitosan, chitosan $+ CoFe_2O_4COOH - MWCNT\ 2\%$,chitosan $+ CoFe_2O_4COOH - MWCNT\ 4\%$,chitosan $+ Fe_3O_4COOH - MWCNT\ 2\%$ and chitosan $+ Fe_3O_4COOH - MWCNT\ 4\%$ were measured and investigated against a series of gases such as CO, CO_2 and O_2. For each experiment, parameters such as the exposure time and the ambient temperature were kept stable.

In the introduction part, some information about the gas sensors, the conducting polymers, a theoretical background, synthesis of the materials (done by Mehmet Şenel at Fatih University) and gases that were used were mentioned. The experimental procedure and gas flow control measurement system were explained in the experimental section. In the last section, QCM measurement results were demonstrated and discussed in details.

The sensor response value of the bare chitosan was obtained as ‰2.96 for CO, but after the modification with $CoFe_2O_4COOH - MWCNT\ 2\%$, the sensor response of chitosan $+ CoFe_2O_4COOH - MWCNT\ 2\%$ material increased to ‰10.05. After the modification with $CoFe_2O_4COOH - MWCNT\ 4\%$, the sensor response of chitosan $+ CoFe_2O_4COOH - MWCNT\ 4\%$ material decreased to ‰8.13.The data that were obtained show us that for the most efficient gas sensor, the ratio of mixtures should be 2% under N_2 gas environment. The sensor response value of the bare Chitosan was obtained as ‰2.96 for CO, but after the modification with $Fe_3O_4COOH - MWCNT\ 4\%$, the sensor response of chitosan $+ Fe_3O_4COOH - MWCNT\ 4\%$ material increased to 9.08 ‰. After the modification with Fe_3O_4COOH-MWCNT 4%, the sensor response of chitosan $+ Fe_3O_4COOH - MWCNT\ 4\%$ material decreased to ‰7.82.The data that were obtained show us that for the most efficient gas sensor, the ratio of mixtures should be 2% under N_2 gas environment.

Under air condition, the sensor response value of the bare Chitosan was obtained as 3.48‰ for CO, but after the modification with $CoFe_2O_4COOH-MWCNT$ 2%, the sensor response of chitosan + $CoFe_2O_4COOH-MWCNT$ 2% material increased to ‰9.72. After the modification with $CoFe_2O_4COOH-MWCNT$ 4%, the sensor response of chitosan + $CoFe_2O_4COOH-MWCNT$ 4% material increased to ‰12.79. This could be a result of a higher ratio of active surface area and an increase in the porousity on the sensing film because of the nanoparticle doping. The sensor response value of the bare chitosan was obtained as 3.48 ‰ for CO, but after the modification with $Fe_3O_4COOH-MWCNT$2%, the sensor response of chitosan + $Fe_3O_4COOH-MWCNT$ 2% material increased to ‰18.88. After the modification with Fe_3O_4COOH-MWCNT 4%, the sensor response of chitosan + $Fe_3O_4COOH-MWCNT$ 4% material decreased to 6.61 ‰. The data that were obtained show us that for the most efficient gas sensor, the ratio of mixtures should be 2% .

The sensor response value of the bare chitosan was obtained as ‰8.13 for CO_2, but after the modification with $CoFe_2O_4COOH-MWCNT$ 2%, the sensor response of chitosan + $CoFe_2O_4COOH-MWCNT$ 2% material decreased to ‰3.00. After the modification with $CoFe_2O_4COOH-MWCNT$ 4%, the sensor response of chitosan + $CoFe_2O_4COOH-MWCNT$ 4% material decreased to ‰7.36. That could be because the molecular structure of the chitosan + $CoFe_2O_4COOH-MWCNT$ 2% thin film surface with the same amount of active sites compared to chitosan. The sensor response against CO increased back to the same sensor response level of chitosan after increased Vol of solution. This could be a result of a higher ratio of active surface area and an increase in the porousity on the sensing film because of the nanoparticle doping. The sensor response value of the bare Chitosan was obtained as ‰8.13 for CO_2, but after the modification with $Fe_3O_4COOH-MWCNT$ 2%, the sensor response of

chitosan $+$ Fe$_3$O$_4$COOH $-$ MWCNT 2% material increased to ‰7.13. After the modification with Fe$_3$O$_4$COOH-MWCNT 4%, the sensor response of chitosan $+$ Fe$_3$O$_4$COOH $-$ MWCNT 4% material decreased to ‰3.86.The data that were obtained show us that for the most efficient gas sensor, the ratio of mixtures should be 2% under N$_2$ gas environment.

Under air condition, the sensor response value of the bare chitosan was obtained as ‰2.92 for CO$_2$, but after the modification with CoFe$_2$O$_4$COOH $-$ MWCNT 2%, the sensor response of chitosan $+$ CoFe$_2$O$_4$COOH $-$ MWCNT 2% material increased to ‰14.48. After the modification with CoFe$_2$O$_4$COOH $-$ MWCNT 4%, the sensor response of Chitosan $+$ CoFe$_2$O$_4$COOH $-$ MWCNT 4% material decreased to ‰14.70. This could be a result of a higher ratio of active surface area and an increase in the porousity on the sensing film because of the nanoparticle doping. The sensor response value of the bare Chitosan was obtained as ‰2.92 for CO$_2$, but after the modification with Fe$_3$O$_4$COOH $-$ MWCNT 2%, the sensor response of chitosan $+$ Fe$_3$O$_4$COOH $-$ MWCNT 2% material increased to ‰27.22. After the modification with Fe$_3$O$_4$COOH-MWCNT 4%, the sensor response of chitosan $+$ Fe$_3$O$_4$COOH $-$ MWCNT4% material decreased to ‰8.12.The data that were obtained show us that for the most efficient gas sensor, the ratio of mixtures should be 2% .

The sensor response value of the bare Chitosan was obtained as ‰1.89 forO$_2$, but after the modification with CoFe$_2$O$_4$COOH $-$ MWCNT 2%, the sensor response of chitosan $+$ CoFe$_2$O$_4$COOH $-$ MWCNT 2% material increased to ‰.13.33 After the modification with CoFe$_2$O$_4$COOH $-$ MWCNT 4%, the sensor response of chitosan $+$ CoFe$_2$O$_4$COOH $-$ MWCNT 4% material decreased to ‰11.75.The data that were obtained show us that for the most efficient gas sensor, the ratio of mixtures should be 2% under N$_2$ gas environment. The sensor response value of the bare chitosan was

obtained as ‰1.89 for O_2, but after the modification with $Fe_3O_4COOH - MWCNT$ 2%, the sensor response of chitosan + $Fe_3O_4COOH - MWCNT$ 2% material increased to ‰6.55. After the modification with Fe_3O_4COOH-MWCNT 4%, the sensor response of chitosan + $Fe_3O_4COOH - MWCNT$ 4% material decreased to ‰5.22. The data that were obtained show us that for the most efficient gas sensor, the ratio of mixtures should be 2% under N_2 gas environment.

Under air condition, the sensor response value of the bare chitosan was obtained as 2.03 ‰ for O_2, but after the modification with $CoFe_2O_4COOH - MWCNT$ 4%, the sensor response of chitosan + $CoFe_2O_4COOH - MWCNT$ 2% material increased to ‰33.63. After the modification with $CoFe_2O_4COOH - MWCNT$ 4%, the sensor response of chitosan + $CoFe_2O_4COOH - MWCNT$ 4% material decreased to ‰11.50. The data that were obtained show us that for the most efficient gas sensor, the ratio of mixtures should be 2%.

The sensor response value of the bare chitosan was obtained as ‰2.03 for O_2, but after the modification with $Fe_3O_4COOH - MWCNT$ 2%, the sensor response of chitosan + $Fe_3O_4COOH - MWCNT$2% material increased to ‰47.50. After the modification with Fe_3O_4COOH-MWCNT 4%, the sensor response of chitosan + $Fe_3O_4COOH - MWCNT$ 4% material decreased to ‰9.96. The data that were obtained show us that for the most efficient gas sensor, the ratio of mixtures should be 2% .

As conclusion, the experimental results that have been obtained in this study showed varying degrees of the sensor responses, which made them easy to use as practical CO sensors thanks to their high sensitive behaviors against the investigated materials which is chitosan + $CoFe_2O_4COOH - MWCNT$ 2%. $CoFe_2O_4COOH - MWCNT$-doped

chitosan, which increases the selectivity against CO, were not studied before as gas sensors in literature so far. Future studies might focus on the functionalization of chitosan with different molecules so as to increase the selectivity properties of the conducting polymers against another specific gas molecule. Also, the experimental results that have been obtained in this study showed varying degrees of the sensor responses, which made them easy to use as practical CO_2 sensors thanks to their high sensitive behaviors against the investigated materials which is $Fe_3O_4COOH - MWCNT\ 2\%$. Fe_3O_4COOH-MWCNT -doped chitosan, which increases the selectivity against CO, were not studied before as gas sensors in literature so far. Future studies might focus on the functionalization of chitosan with different molecules so as to increase the selectivity properties of the conducting polymers against another specific gas molecule. Finally, the experimental results that have been obtained in this study showed varying degrees of the sensor responses, which made them easy to use as practical O_2 sensors thanks to their high sensitive behaviors against the investigated materials which is $Fe_3O_4COOH - MWCNT2\%$. Fe_3O_4COOH-MWCNT -doped chitosan, which increases the selectivity against CO, were not studied before as gas sensors in literature so far. Future studies might focus on the functionalization of chitosan with different molecules so as to increase the selectivity properties of the conducting polymers against another specific gas molecule.

The data that were obtained show us that for the most efficient gas sensor, the ratio of mixtures should be 2%. That proves us that optimum working efficiency is that ratio. While this is the case in nitrogen environment, it was different in the air environment. Only Fe mixtures give the optimum results of 2%.

Since chitosan is a non-conductive material and it also makes other materials mounted on it non-conductive, no electrical results were obtained in this study.

References

1. **Yamazoe, N.**, (2005). *Toward innovations of gas sensor technology.* Sensors and Actuators B: Chemical, **108**(1): p. 2-14.

2. **Taylor, R.F. and J.S. Schultz**, (2010). *Handbook of chemical and biological sensors*. CRC Press.

3. **Fine, G.F., et al.**, (2010). *Metal oxide semi-conductor gas sensors in environmental monitoring.* Sensors, **10**(6): p. 5469-5502.

4. **Yamazoe, N.**, (2005). *Toward innovations of gas sensor technology.* Sensors and Actuators B: Chemical, **108**(1–2): p. 2-14.

5. **Ram, M.K., et al.**, (2005). *CO gas sensing from ultrathin nano-composite conducting polymer film.* Sensors and Actuators B: Chemical, **106**(2): p. 750-757.

6. **Ando, M., T. Kobayashi, and M. Haruta**, (1997). *Combined effects of small gold particles on the optical gas sensing by transition metal oxide films.* Catalysis Today, **36**(1): p. 135-141.

7. **Ando, M., R. Chabicovsky, and M. Haruta**, (2001). *Optical hydrogen sensitivity of noble metal–tungsten oxide composite films prepared by sputtering deposition.* Sensors and Actuators B: Chemical, **76**(1): p. 13-17.

8. **Di Natale, C., et al.**, (1998). *Characterization and design of porphyrins-based broad selectivity chemical sensors for electronic nose applications.* Sensors and Actuators B: Chemical, **52**(1): p. 162-168.

9. **Zhu, C., et al.**, (2006). *A precise sensor for SF 6 based on piezoelectric ultrasound.* Xiyou Jinshu Cailiao yu Gongcheng(Rare Metal Materials and Engineering), **35**: p. 157-158.

10. **Yamamoto, O., T. Takuma, and M. Kinouchi**, (2002). *Recovery of SF/sub 6/from N/sub 2//SF/sub 6/gas mixtures by using a polymer membrane.* Electrical Insulation Magazine, IEEE, **18**(3): p. 32-37.

11. **Wongchoosuk, C., et al.**, (2010). *Multi-walled carbon nanotube-doped tungsten oxide thin films for hydrogen gas sensing.* Sensors, **10**(8): p. 7705-7715.

12. **Wang, Y., et al.**, (2010). *Improving the performance of catalytic combustion type methane gas sensors using nanostructure elements doped with rare earth cocatalysts.* Sensors, **11**(1): p. 19-31.

13. **Vashpanov, Y., H. Choo, and D.S. Kim**, (2011). *Dynamic control of adsorption sensitivity for photo-EMF-based ammonia gas sensors using a wireless network.* Sensors, **11**(11): p. 10930-10939.

14. **Tong, L., et al.** (2004). *Oil-gas separation mechanism of polymer membranes applied to online transformer dissolved gases monitoring.* in *Electrical Insulation, 2004. Conference Record of the 2004 IEEE International Symposium on.* IEEE.

15. **Minglei, S., et al.** (2010). *Gas concentration detection using ultrasonic based on wireless sensor networks.* in *Information Science and Engineering (ICISE), 2010 2nd International Conference on.* IEEE. 6

16. **Manzoli, A., et al.**, (2011). *Low-cost gas sensors produced by the graphite line-patterning technique applied to monitoring banana ripeness.* Sensors, **11**(6): p. 6425-6434.

17. **Liu, J., et al.**, (2011). *Advances in SAW gas sensors based on the condensate-adsorption effect.* Sensors, **11**(12): p. 11871-11884.

18. **Kulinyi, S., et al.**, (2005). *Olfactory detection of methane, propane, butane and hexane using conventional transmitter norms.* Sensors and Actuators B: Chemical, **111**: p. 286-292.

19. **Huyen, D.N., et al.**, (2011). *Effect of TiO2 on the gas sensing features of TiO2/PANi nanocomposites.* Sensors, **11**(2): p. 1924-1931.

20. **Duval, M.**, (2003). *New techniques for dissolved gas-in-oil analysis.* Electrical insulation magazine, IEEE, **19**(2): p. 6-15.

21. **Ding, W., et al.**, (2006). *Calibration methods of carbon nanotube gas sensor for partial discharge detection in SF/sub 6.* Dielectrics and Electrical Insulation, IEEE Transactions on, **13**(2): p. 353-361.

22. **Chinvongamorn, C., et al.**, (2008). *Amperometric determination of sulfite by gas diffusion-sequential injection with boron-doped diamond electrode.* Sensors, **8**(3): p. 1846-1857.

23. **Chen, D., S. Lei, and Y. Chen**, (2011). *A single polyaniline nanofiber field effect transistor and its gas sensing mechanisms.* Sensors, **11**(7): p. 6509-6516.

24. **Changping, Z., et al.**, (2005). *Microconcentration detector for SF6 based on CPLD.* Chinese Journal of Scientific Instrument, **26**(8): p. 448-449.

25. **Chang, Y.-C., et al.**, (2011). *Bromocresol green/mesoporous silica adsorbent for ammonia gas sensing via an optical sensing instrument.* Sensors, **11**(4): p. 4060-4072.

26. **Catalan, L.J., V. Liang, and C.Q. Jia**, (2006). *Comparison of various detection limit estimates for volatile sulphur compounds by gas chromatography with pulsed flame photometric detection.* Journal of chromatography A, **1136**(1): p. 89-98.

27. **Anderson, T., et al.**, (2009). *Advances in hydrogen, carbon dioxide, and hydrocarbon gas sensor technology using GaN and ZnO-based devices.* Sensors, **9**(6): p. 4669-4694.

28. **Tardy, P., et al.**, (2004). *Dynamic thermal conductivity sensor for gas detection.* Sensors and Actuators B: Chemical, **98**(1): p. 63-68.

29. **Sonoyama, M., Y. Kato, and H. Fujita**. (2010). *Application of ultrasonic to a hydrogen sensor*. in *Sensors, 2010 IEEE*. IEEE.

30. **Miya, H., et al.** (2009). *Compact Raman Lidar for hydrogen gas leak detection*. in *Conference on Lasers and Electro-Optics/Pacific Rim*. Optical Society of America.

31. **Marr, I., et al.**, (2011). *Planar zeolite film-based potentiometric gas sensors manufactured by a combined thick-film and electroplating technique.* Sensors, **11**(8): p. 7736-7748.

32. **Koplin, T.J., et al.**, (2006). *Workflow for high throughput screening of gas sensing materials.* Sensors, **6**(4): p. 298-307.

33. **Iannotta, S., et al.** (2008). *Novel Nano-Hybrid gas sensor based on n-TiO2 functionalized by phthalocyanines via supersonic beam co-deposition: performance and application to automotive air quality*. in *Sensors, 2008 IEEE*. IEEE.

34. **Ho, K.-C., W.-T. Hung, and J.-C. Yang**, (2003). *On the Electrooxidation and amperometric detection of no gas at the pt/nafion® electrode.* Sensors, **3**(8): p. 290-303.

35. **Haiming, Z.** (2008). *Experiment Study of continuous emission monitoring system based on Differential Optical Absorption Spectroscopy*. in *Education Technology and Training, 2008. and 2008 International Workshop on Geoscience and Remote Sensing. ETT and GRS 2008. International Workshop on*. IEEE.

36. **Frodl, R. and T. Tille**, (2006). *A high-precision NDIR gas sensor for automotive applications.* IEEE Sensors Journal, **6**(6).

37. **Fleming, W.J.**, (2001). *Overview of automotive sensors.* Sensors Journal, IEEE, **1**(4): p. 296-308.

38. **Endres, H.-E., et al.**, (1996). *A thin-film SnO< sub> 2</sub> sensor system for simultaneous detection of CO and NO< sub> 2</sub> with neural signal evaluation.* Sensors and Actuators B: Chemical, **36**(1): p. 353-357.

39. **Caucheteur, C., et al.**, (2008). *Catalytic fiber Bragg grating sensor for hydrogen leak detection in air.* Photonics Technology Letters, IEEE, **20**(2): p. 96-98.

40. **Billi, E., et al.**, (2002). *Development of a protected gas sensor for exhaust automotive applications.* Sensors Journal, IEEE, **2**(4): p. 342-348.

41. **Belov, I., et al.** (2004). *Thermal and flow analysis of SiC-based gas sensors for automotive applications*. in *Thermal and Mechanical Simulation and Experiments in Microelectronics and Microsystems, 2004. EuroSimE 2004. Proceedings of the 5th International Conference on*. IEEE.

42. **Tamaekong, N., et al.**, (2010). *Flame-spray-made undoped zinc oxide films for gas sensing applications.* Sensors, **10**(8): p. 7863-7873.

43. **Yi, W., et al.** (2009). *Measurement of CH4 by differential infrared optical absorption spectroscopy*. in *Electronic Measurement & Instruments, 2009. ICEMI'09. 9th International Conference on*. IEEE.

44. **Xiao, G., et al.** (2011). *Trace amount formaldehyde gas detection for indoor air quality monitoring*. in *Instrumentation and Measurement Technology Conference (I2MTC), 2011 IEEE*. IEEE.

45. **Kim, S.-J., et al.**, (2011). *Design of selective gas sensors using additive-loaded In2O3 hollow spheres prepared by combinatorial hydrothermal reactions.* Sensors, **11**(11): p. 10603-10614.

46. **Kim, K.-S., et al.**, (2010). *A nanopore structured high performance toluene gas sensor made by nanoimprinting method.* Sensors, **10**(1): p. 765-774.

47. **Ke, M.-T., et al.**, (2009). *A MEMS-based benzene gas sensor with a self-heating wo3 sensing layer.* Sensors, **9**(4): p. 2895-2906.

48. **Yeung, C.S., Y.K. Chen, and Y.A. Wang**, (2011). *Defected and Substitutionally Doped Nanotubes: Applications in Biosystems, Sensors, Nanoelectronics, and Catalysis.*

49. **Richardson, T., et al.**, (2006). *The NO_2 gas sensing properties of calixarene/porphyrin mixed LB films.* Colloids and Surfaces A: Physicochemical and Engineering Aspects, **284**: p. 320-325.

50. **Yamazoe, N. and K. Shimanoe**, (2008). *Theory of power laws for semiconductor gas sensors.* Sensors and Actuators B: Chemical, **128**(2): p. 566-573.

51. **Kanan, S.M., et al.**, (2009). *Semiconducting metal oxide based sensors for selective gas pollutant detection.* Sensors, **9**(10): p. 8158-8196.

52. **Wang, C., et al.**, (2010). *Metal oxide gas sensors: sensitivity and influencing factors.* Sensors, **10**(3): p. 2088-2106.

53. Gas sensors: A review - Scientific Figure on ResearchGate. Available from: https://www.researchgate.net/285988329_fig9_Fig-7-Showing-one-electrode-configuration-of-semiconductor-gas-sensor-40 [accessed 9 Oct, 2016]

54. **Chou, J.**, (2000). *Hazardous gas monitors: a practical guide to selection, operation and applications.* McGraw-Hill Professional.

55. **Lee, S.-H., et al.**, (2005). *Rapid detection of bacterial spores using a quartz crystal microbalance (QCM) immunoassay.* Sensors Journal, IEEE, **5**(4): p. 737-743.

56. **Albert, K.J., et al.**, (2000). *Cross-reactive chemical sensor arrays.* Chemical Reviews, **100**(7): p. 2595-2626.

57. . **Lu, X., et al.**, (2011). *One-dimensional conducting polymer nanocomposites: Synthesis, properties and applications.* Progress in Polymer Science, **36**(5): p. 671-712.

58. **Sauerbrey, G.**, (1959). *Verwendung von Schwingquarzen zur Wägung dünner Schichten und zur Mikrowägung.* Zeitschrift für Physik, **155**(2): p. 206-222.

59. **Buck, R.P., et al.**, (2004). *Piezoelectric chemical sensors - (IUPAC Technical Report).* Pure and Applied Chemistry, **76**(6): p. 1139-1160.

60. **Janshoff, A., H.J. Galla, and C. Steinem**, (2000). *Piezoelectric mass-sensing devices as biosensors - An alternative to optical biosensors?* Angewandte Chemie-International Edition, **39**(22): p. 4004-4032.

61. **Hunt, W.D., D.D. Stubbs, and S.-H. Lee**, (2003). *Time-dependent signatures of acoustic wave biosensors.* Proceedings of the IEEE, **91**(6): p. 890-901.
97. **Corso, C.D., et al.**, (2006). *Real-time detection of mesothelin in pancreatic cancer cell line supernatant using an acoustic wave immunosensor.* Cancer Detection and Prevention, **30**(2): p. 180-187.

62. **Sauerbrey, G.**, (1959). *Use of quartz vibration for weighing thin films on a microbalance.* J. Physik, **155**: p. 206-212.

63. **Janata, J.**, (2009). *Principles of chemical sensors*. Springer.

64. **Bottom, V.E.**, (1982). *Introduction to quartz crystal unit design*. Van Nostrand Reinhold New York.

65. **List, E.J.W., et al.**, (2002). *The Effect of Keto Defect Sites on the Emission Properties of Polyfluorene-Type Materials.* Advanced Materials, **14**(5): p. 374-378.

66. **Johannsmann, D.**, (2001). *Derivation of the shear compliance of thin films on quartz resonators from comparison of the frequency shifts on different harmonics: A perturbation analysis.* Journal of Applied Physics, **89**(11): p. 6356-6364. 65

67. **Gomes, M., P.S.T. Nogueira, and J.A. Oliveira**, (2000). *Quantification of CO$_2$, SO$_2$, NH$_3$, and H$_2$S*

with a single coated piezoelectric quartz crystal. Sensors and Actuators B: Chemical, **68**(1): p. 218-222.

68. **Glassford, A.**, (1978). *Response of a quartz crystal microbalance to a liquid deposit.* Journal of Vacuum Science and Technology, **15**(6): p. 1836-1843.

69**. Osada Y, DeRossi DE (eds),** (2000) Polymer sensors and actuators. Springer, Berlin

70**. Gaines GL Jr,** (1966) Insoluble monolayers at liquid-gas interfaces. Wiley-Interscience, New York, NY

71. **Schmitt K, Hoffmann C** ,(2010) High-refractive-index waveguide platforms for chemical and biosensing. In: **Zourob M, Lakhtakia A (eds),** Chemical sensors and biosensors: methods and applications. Springer, Berlin, pp 21–54

72. **Syms RRA, Cozens JR,** (1993) Optical guided waves and devices. Academic, London

73. **Korishko YN, Fedorov VA, Feoktistova OY,** (2000) LiNbO 3 optical waveguide fabrication by high-temperature proton exchange. J Lightwave Technol 18:562–568

74. **Hu H, Lu F, Chen F, Shi B-R, Wang K-M, Shen D-Y,** (2001) Monomode optical waveguide in lithium niobate formed by MeV Si + ion implantation. J Appl Phys 89:5224–5226

75. **Worhoff K, Lambeck PV, Driessen A,** (1999) Design, tolerance analysis, and fabrication of silicon oxynitride based planar optical waveguides for communication devices. J Lightwave Technol 17:1401–1407

76. **Lalauze, R.**, (2010). *Adsorption Phenomena*, in *Physical Chemistry of Solid-Gas Interfaces*. 2010, ISTE. p. 1-27.

77. **Unal, B., M. Senel, A. Baykal and H. Sözeri** (2013). "Multiwall-carbon nanotube/cobalt ferrite hybrid: Synthesis, magnetic and conductivity characterization." <u>Current Applied Physics</u> **13**(7): 1404-1412.

78. **T.A. Saleh, S. Agarwal, V.K. Gupta** (2011), Synthesis of MWCNT/MnO2 and their application for simultaneous oxidation of arsenite and sorption of arsenate, Appl. Catal. B 106 46e53.

79. **Baykal, A., M. Senel, B. Unal, E. Karaoğlu, H. Sözeri and M. S. Toprak** (2013). "Acid

functionalized multiwall carbon nanotube/magnetite (MWCNT)-COOH/Fe3O4 hybrid: synthesis, characterization and conductivity evaluation." Journal of Inorganic and Organometallic Polymers and Materials 23(3): 726-735.

80**. Y. Liu, L. Gao, Carbon 43, 47** (2005)

81. **J. Jang, J. Bae, S. Yoon, J. Mater. Chem. 13, 676** (2003)

82. **J. Zhang, H. Zou, Q. Qing, Y. Yang, Q. Li, Z. Liu, X. Guo, Z. Du,** J. Phys. Chem. B 107, 3712 (2003)

83.**B. Unal, Z. Durmus, H. Kavas, A. Baykal, M.S. Toprak**, Mater. Chem. Phys. 123, 184 (2010)

84**. B. Unal, Z. Durmus, A. Baykal, H. Sozeri, M.S. Toprak, L. Alpsoy, J. Alloy**. Compd. 505, 172 (2010)

85. **B. Unal, A. Baykal, M. Senel, H. Sozeri**, Synthesis and characterization of multiwall-

carbon nanotubes decorated with nickel ferrite hybrid, J Inorg Organomet Polym. doi 10.1007/s10904-012-9803-8

86. **Younes, I. and M. Rinaudo** (2015). "Chitin and chitosan preparation from marine sources. Structure, properties and applications." Marine drugs **13**(3): 1133-1174.
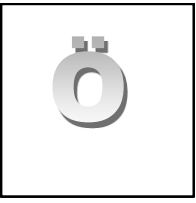
CURRICULUM VITAE

Name Surname	**: Uğur ACAR**
Place and Date of Birth	**: IZMIR / 21.05.1989**
E-Mail	**: uguracar@yandex.com**

EDUCATION **:**

- **B.Sc.** **: 2012, Ege University, Faculty of Scienc, Physics**